Enhanced distribution of NK012, a polymeric micelle-encapsulated SN-38, and sustained release of SN-38 within tumors can beat a hypovascular tumor

Yohei Saito,[1,2] Masahiro Yasunaga,[1] Junichiro Kuroda,[1] Yoshikatsu Koga[1] and Yasuhiro Matsumura[1,3]

[1]Investigative Treatment Division, Center for Innovative Oncology, National Cancer Center Hospital East, 6-5-1 Kashiwanoha, Kashiwa, Chiba 277-8577; [2]Laboratory of Cancer Biology, Department of Integrated Biosciences, Graduate School of Frontier Sciences, The University of Tokyo, 5-1-5 Kashiwanoha, Kashiwa, Chiba 277-8562, Japan

(Received January 16, 2008/Revised February 14, 2008/Accepted February 14, 2008/Online publication April 21, 2008)

Human pancreatic cancer is generally hypovascular in nature and rich in interstitium. These pathological barriers may contribute to the intractable nature of pancreatic cancer by binding the penetration of anticancer agents throughout the tumor tissue. The aim of the present study was to determine whether NK012 is an appropriate formulation for the treatment of hypovascular tumors. Among pancreatic tumor xenografts, PSN1 appeared to have the richest tumor vasculature and the least number of stromal cells and matrix. In contrast, Capan1 had the poorest tumor vasculature and most abundant stromal tissue. Fluorescence microscopy and high-performance liquid chromatography analysis demonstrated that although NK012 accumulated and continued to be distributed for more than 48 h throughout the entire body of both tumors, CPT-11 disappeared almost entirely from both tumors within 6 h. In addition, efficient sustained release of SN-38 was maintained for more than 96 h in both tumors following administration of NK012. Following the administration of CPT-11, SN-38 was no longer detectable after 24 h in the Capan1 tumor or after 48 h in the PSN1 tumor. All tumors were eradicated in the mice treated with NK012 but not in those treated with CPT-11. Because the antitumor activity of SN-38 is time dependent, NK012, which combines enhanced distribution with sustained release of SN-38 within tumors, may be ideal for the treatment of hypovascular tumors, such as pancreatic cancer. (*Cancer Sci* 2008; 99: 1258–1264)

Pancreatic cancer has one of the worst prognoses among cancers.[1] The median survival of cases of advanced pancreatic cancer is only approximately one in two 1 year after systemic gemcitabine-based chemotherapy.[2] The recent success of molecular-targeting agents has also had some impact on pancreatic cancer treatment. A recent phase III trial of gemcitabine alone versus gemcitabine plus erlotinib (a tyrosine kinase inhibitor) in patients with advanced pancreatic cancer showed that overall survival was significantly prolonged in the gemcitabine + erlotinib arm. However, median survival in the gemcitabine + erlotinib arm (6.24 months) was only 10 days longer than in the gemcitabine-alone arm (5.91 months).[3] There is therefore an urgent need to develop modalities by which cytotoxic drugs can exert their significant antitumor activity to their full potential and reasonably prolong the overall survival of patients with advanced pancreatic cancer. There may be several reasons why pancreatic cancer is intractable. It is conceivable that anticancer agents are not delivered efficiently enough to the pancreatic cancer cells to kill them. Pancreatic cancer tissue is generally hypovascular in nature,[4,5] and is rich in stromal cells and extracellular matrix, and these pathological barriers may hinder efficient penetration of the anticancer agents throughout the entire body of the pancreatic cancer.

The role of drug delivery systems (DDS) is to selectively deliver cytotoxic drugs to tumor tissues while lessening their distribution to normal tissues in order to reduce their side effects.[6–8] However, it is conceivable that satisfactory drug delivery cannot be achieved in cancers having very few tumor vessels and an abundant collagen-rich interstitium. Therefore, a more sophisticated DDS may be needed for efficient delivery of drugs to such types of cancer as pancreatic cancer.

SN-38, a biologically active metabolite of irinotecan hydrochloride (CPT-11), has potent antitumor activity but has not been used clinically because of its water insolubility. NK012, a successful drug formulation composed of SN-38-incorporating polymeric micelles, has been developed recently, and the remarkable antitumor effects of NK012 against the human small cell lung cancer SBC-3, especially the vascular endothelial growth factor (VEGF)-secreting SBC-3–VEGF tumor, has been demonstrated.[8]

In the present study, we clarified the relationship between the tumor vasculature and interstitium using several human pancreatic xenografts, and evaluated the therapeutic effect of NK012 in a hypovascular and hypervascular pancreatic tumor.

Materials and Methods

Drugs and cells. SN-38 and NK012 were synthesized by Nippon Kayaku (Tokyo, Japan). CPT-11 was purchased from Yakult (Tokyo, Japan). The human pancreatic cancer cell lines Panc1, PSN1, BxPC3, and Capan1 were purchased from American Type Culture Collection (Rockville, MD, USA).

Panc1, PSN1, and Capan1 were maintained in Dulbecco's modified Eagle's medium (DMEM) supplemented with 10% fetal bovine serum, streptomycin, and L-glutamine (Sigma, St Louis, MO, USA) in atmosphere of 5% CO_2 at 37°C. BxPC3 were maintained in RPMI-1640 supplemented with 10% fetal bovine serum, streptomycin, and L-glutamine (Sigma) in an atmosphere of 5% CO_2 at 37°C.

Experimental mouse model. Female BALB/c nude mice, 6 weeks old, were purchased from CLEA Japan (Tokyo, Japan). Mice were inoculated subcutaneously in the flank with 1×10^7 cells/300 μL phosphate-buffered saline (PBS). All animal procedures were carried out in compliance with the guidelines for the care and use of experimental animals, laid down by the Committee for Animal Experimentation of the National Cancer Center; these guidelines meet the ethical standards required by law and also comply with the guidelines for the use of experimental animals in Japan.

[3]To whom correspondence should be addressed. E-mail: yhmatsum@east.ncc.go.jp

doi: 10.1111/j.1349-7006.2008.00806.x

Immunohistochemical study of various human pancreatic tumor xenografts. When the tumor volume reached 300 mm^3, tumors were excised from the mice and used for immunohistochemical analysis. To stain the blood vessels, the tissues were embedded in Optimal Cutting Temperature Compound (Sakura Finetechnochemical, Tokyo, Japan) and frozen at –80°C until use. Six micrometer-thick tumor sections were prepared using a cryostatic microtome, Tissue-Tek Cryo3 (Sakura Finetechnochemical), and then air dried for 1 h. The sections were soaked in 10% formalin for 15 min, and washed three times with 0.2 M PBS. The sections were then rinsed with ultrapure water. Endogeneous peroxidase was blocked with a 0.3% hydrogen peroxide solution in 100% methanol for 20 min. The sections were then rinsed three times with PBS for 3 min each. Non-specific protein binding was blocked with 5% skim milk (BD, Franklin Lakes, NJ, USA) in PBS for 30 min at room temperature. After draining off the skim milk solution, a polyclonal antibody against factor VIII (Zymed Laboratories, South San Francisco, CA, USA) was added at a dilution of 1:50, followed by incubation for 1 h and three rinses with PBS for 5 min each. Biotinylated antirabbit IgG was added at a dilution of 1:50, followed by incubation for 1 h. The sections were rinsed three times with PBS, and Vectastain Elite ABC Reagent (Vector Laboratories, Burlingame, CA, USA) was added for 30 min. The sections were rinsed again three times with PBS and incubated with the 3,3′-diaminobenzidine tetrahydrochloride (DAB+) Liquid System (Dako, Glostrup, Denmark) for 30 s. Finally, the sections were rinsed and counterstained with hematoxylin solution. For staining of type I, III, and IV collagen, tissues were fixed with 4% formalin, and the paraffin sections were prepared by the Tokyo Histopathologic Laboratory (Tokyo, Japan). First, the sections were soaked three times for 5 min each in xylene, and then three times for 3 min each in ethanol to remove the paraffin. The sections were then rinsed with ultrapure water and endogeneous peroxidase was blocked with a 0.3% hydrogen peroxide solution in 100% methanol for 20 min, followed by three rinses for 5 min with PBS. Then, Proteinase K (Dako) was added. After the sections were rinsed three times for 5 min each with 0.2 M PBS, non-specific protein binding was blocked with a 1% normal goat serum (Dako) solution in PBS for 30 min at room temperature. Then, after three rinses for 5 min each with PBS, polyclonal rabbit anti type I, III, and IV collagen antibodies (Dako) were added at dilutions of 1:500 (type I collagen), 1:10 000 (type III collagen), and 1:2000 (type IV collagen), followed by incubation for 1 h. The slides were rinsed in PBS and incubated for 30 min with Envision/HRP (Dako) directed against the primary antibody. After further rinsing, the sections were incubated with the DAB+ Liquid System (Dako) for 30 s. Then, after a final rinse, the sections were counterstained with hematoxylin solution.

***In vitro* growth assay.** The growth-inhibitory effects of NK012, SN-38, and CPT-11 were examined using the WST8 assay. Cell suspensions (5000 cells/100 μL) were seeded into a 96-well microliter plate, which was incubated for 24 h at 37°C. Then, after removal of the medium, 100 μL of medium containing various concentrations of each drug was added to the wells, which were then incubated for 48 h at 37°C. After removal of the medium, 10 μL of WST8 solution and 90 μL of medium were added to the wells, followed by incubation for 4 h at 37°C. The growth-inhibitory effect of each drug was assessed spectrophotometrically (SpectraMax 190; Molecular Devices, Sunnyvale, CA, USA).

Distribution studies of CPT-11 and NK012 in the tumors by fluorescence microscopy. Nude mice bearing PSN1, as a hypervascular tumor model, or Capan1, as a hypovascular tumor model, were used for studying the distribution of NK012 and CPT-11, when the tumors reached 300 mm^3 in volume. The maximum tolerated dose (MTD) of NK012 (30 mg/kg) or CPT-11 (66.7 mg/kg) was injected intravenously into the mice. At 1, 6, 24, or 48 h after the injection of NK012 or CPT-11, the mice were administered fluorescein-labeled *Lycopersicon esculentum* lectin (100 μL/mouse) (Vector Laboratories) for the purpose of visualizing the tumor blood vessels. The tumors were then excised and embedded in Optimal Cutting Temperature Compound and frozen at –80°C before 6 μm-thick sections were prepared using Tissue-Tek Cryo3. The frozen sections were examined under a fluorescence microscope, Biorevo (Keyence, Osaka, Japan), at an excitation wavelength of 377 nm and emission wavelength 447 nm in order to evaluate the distribution of CPT-11 and NK012 within the tumor tissues. Because formulations containing SN-38 bound via ester bonds possess a particular fluorescence, both CPT-11 and NK012 were detected under the same fluorescence conditions.

Distribution studies of free SN-38, CPT-11, and NK012 in the tumors by high-performance liquid chromatography. When PSN1 and Capan1 tumors reached 300 mm^3 in volume, NK012 (30 mg/kg) or CPT-11 (66.7 mg/kg) was administered intravenously to the mice. At 1, 6, 24, 72, or 96 h after the injection of NK012 and CPT-11, each tumor was excised. The tumor tissues were rinsed with physiological saline, mixed with 0.1 M glycine-HCl buffer (pH 3.0) in methanol at 5% (w/w) and homogenized. To detect free SN-38 and CPT-11, the tumor samples (100 μL) were mixed with 20 μL of 1 mM phosphoric acid in methanol (1:1), 40 μL ultrapure water, and camptothecin was used as the internal standard (10 ng/mL for free SN-38, 15 ng/mL for CPT-11). The samples were vortexed vigorously for 10 s and filtered through Ultrafree-MC Centrifugal Filter Devices (Millipore, Bedford, MA, USA). Reverse-phase high-performance liquid chromatography (HPLC) was conducted at 35°C on a Mightysil RP-18 GP column (150 × 4.6 mm; Kanto Chemical, Tokyo, Japan). The samples were injected into an Alliance Water 2795 HPLC system (Waters, Milford, MA, USA) equipped with a Waters 2475 multi λ fluorescence detector. The detector was set at 365 and 430 nm (excitation and emission wavelengths, respectively) for CPT-11, and at 365 and 540 nm for SN-38.

For polymer-bound SN-38 detection, SN-38 was released from the conjugate as described previously.[8] In brief, 100 μL tissue samples were diluted with 20 μL methanol (50% [w/w]) and 20 μL NaOH (0.7 M). The samples were incubated for 15 min at room temperature. After incubation, 20 μL HCl (0.7 M) and 60 μL of internal standard solution was added to the samples, and then the hydrolysate was filtered. The filtrate was applied to the HPLC system.

Polymer-bound SN-38 was determined by subtraction of non-polymer-bound SN-38 from the total SN-38 in the hydrolysate.

Antitumor activity of NK012 and CPT-11 against Capan1 or PSN1 xenografts. When the tumor volume reached approximately 300 mm^3 in volume, the mice were divided randomly into test groups consisting of five mice per group (day 0). The drugs were administered on days 0, 4, and 8 by intravenous injection into the tail vein. NK012 was given at a dose of 30 mg/kg (MTD) and CPT-11 was given at a MTD of 66.7 mg/kg as indicated in the optimal schedule reported previously.[9]

The length (L) and width (W) of the tumor mass were measured every 3 days. The tumor volume (TV) was calculated as follows: $TV = (L \times W^2) \times 0.5233$.

Statistical analysis. Student's *t*-test was used for the statistical analyses. $P < 0.05$ was considered to denote statistical significance.

Results

Density of collagen and the number of tumor blood vessels in the various human pancreatic tumor xenografts. We examined the density of collagen in four pancreatic cancer xenografts (Fig. 1a). Type I collagen was present in the greatest abundance in Capan1 and was least abundance in PSN1. The density of type I collagen in Panc1 and BxPC3 was in second and third place, respectively.

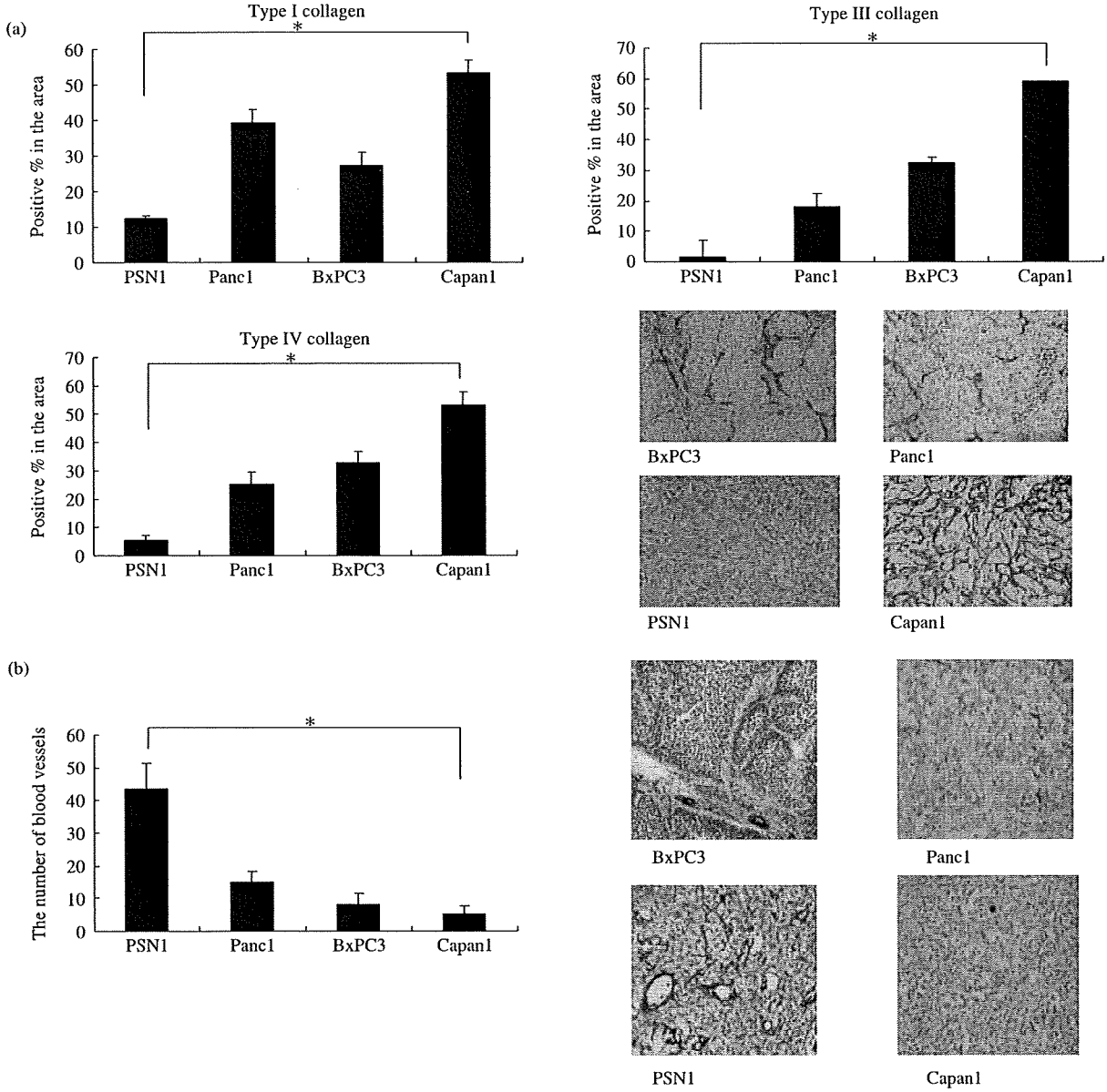

Fig. 1. Examination of the amount of stroma and the number of tumor blood vessels in four human pancreatic cancer xenografts. (a) The amount of stroma in the four xenografts BxPC3, Panc1, PSN1, and Capan1. Immunohistochemical staining was conducted in order to determine the distribution of type I, III, and IV collagen in the tumors. The area occupied by each of type I collagen (left, upper), type III collagen (right, upper), and type IV collagen (left, bottom) was quantified. A representative immunostained image for type IV collagen is shown (right, bottom). (b) The number of blood vessels in the four xenografts. After immunostaining with anti-factor VIII antibody, the number of tumor blood vessels in each of the xenografts was counted. $*P < 0.05$. Bar = SD.

Capan1 exhibited the highest density of type III collagen, and BxPC3 and PSN1 were in second and fourth place, respectively, with respect to the density of type III collagen. The distribution of type IV collagen tended to be similar to that of type I and III collagen.

We also examined the number of tumor blood vessels (Fig. 1b). The PSN1 tumor possessed the largest number of blood vessels among the tumors. In contrast, the Capan1 xenografts had the smallest number of tumor blood vessels.

We have summarized the results on collagen density and blood vessel number obtained in our study for each pancreatic xenograft. Capan1 was the most collagen-rich tumor, and the density of collagen was lowest in PSN1. In contrast, tumor blood vessels were most abundant in PSN1 and least abundant in Capan1. Therefore, we decided to use Capan1 as a hypovascular tumor model and PSN1 as a hypervascular tumor model.

***In vitro* cytotoxic effects of NK012, SN-38, and CPT-11 against the Capan1 and PSN1 cell lines.** The 50% inhibitory concentration (IC_{50}) values of NK012 for the two cell lines, Capan1 (Fig. 2a) and PSN1 (Fig. 2b), ranged from 0.001 to 0.1 μM. NK012 exhibited a remarkably higher cytotoxic effect against both of the cell lines compared with CPT-11. In contrast the cytotoxic effect of SN-38 was similar to that of NK012. The IC_{50} value of each drug against PSN1 was almost similar to that of Capan1.

Antitumor activity analysis of NK012 and CPT-11 using Capan1- and PSN1-bearing nude mice. Antitumor activity was observed in mice treated with NK012 at a dose of 30 mg/kg/d and CPT-11

doi: 10.1111/j.1349-7006.2008.00806.x

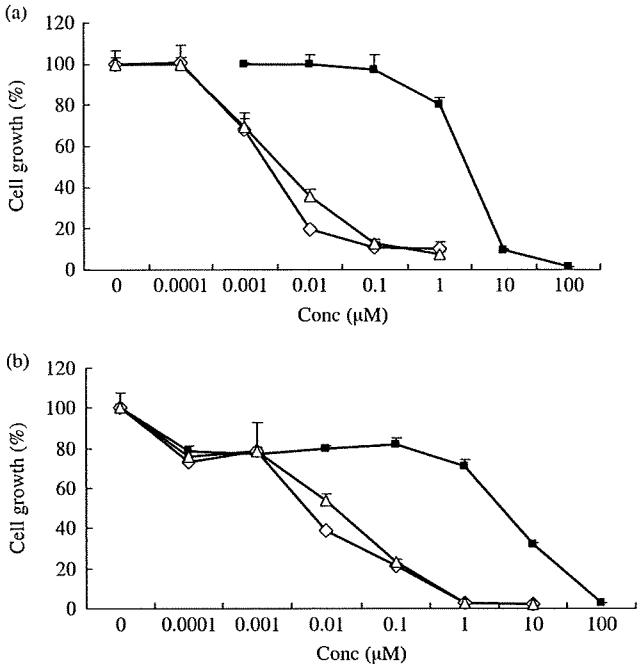

Fig. 2. (a) Capan1 and (b) PSN1 cells were exposed to the indicated concentrations of each drug for 72 h. The growth inhibition curves for NK012 (△), SN-38 (◇), and CPT-11 (■) are shown.

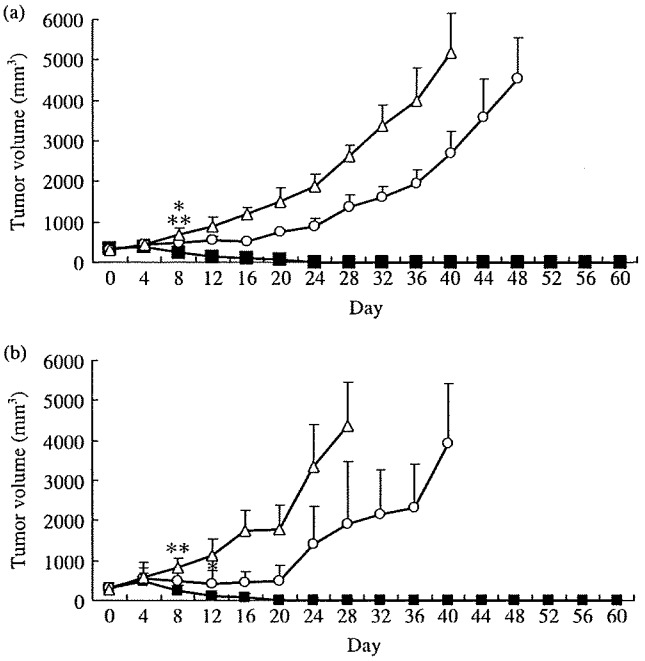

Fig. 3. Antitumor effect of NK012 and CPT-11. NK012 (■), CPT-11 (○), or saline (△) was administered intravenously. When the mean tumor volumes reached 300 mm³ (on day 0), NK012 (30 mg/kg/day) or CPT-11 (66.7 mg/kg/day) was administered on days 0, 4, and 8. Each group consisted of five mice. (a) Capan1 tumor; (b) PSN1 tumor. $*P < 0.05$ (NK012 vs CPT11); $**P < 0.05$ (NK012 vs saline).

at a dose of 66.7 mg/kg/d *in vivo* (Fig. 3). Although CPT-11 exerted a significant antitumor effect compared with the control group in mice bearing the Capan1 tumor, the tumor volume continued to increase consistently. However, in the mice treated with NK012, the tumor volume started to shrink on day 8, and the disappeared completely by day 28 in all treated mice bearing the Capan1 tumor.

In contrast to the observations for the Capan1 tumor, mice bearing the PSN1 tumor treated with CPT-11 showed a slight reduction in tumor volume from day 4 to 12. However, after day 12 the tumor volume began to increase again. On the other hand, the tumor disappeared completely in all mice bearing the PSN1 tumor treated with NK012.

Distribution studies of CPT-11 and NK012 in the solid Capan1 and PSN1 tumors. With the purpose of evaluating drug distribution and accumulation over time, sections of the tumor treated with NK012 or CPT-11 were examined by fluorescence microscopy. Also, we examined the number of tumor blood vessels. In sections of the Capan1 tumor treated with CPT-11, maximum drug accumulation was observed within 1 h of the injection of CPT-11 (Fig. 4a). At 6 h after the injection, the fluorescence originating from CPT-11 had almost entirely disappeared. Subsequently, no accumulation of CPT-11 was observed within the tumor tissues. However, in sections of the Capan1 tumor treated with NK012, fluorescence from NK012 began to appear around tumor blood vessels at 1 h after the intravenous injection and lasted until 48 h. After 6 h, the fluorescent area began to increase and the maximum fluorescence area was observed at 24 h after the injection. Similar results were obtained for the PSN1 tumor (Fig. 4b).

These microscopic observations were confirmed quantitatively by measuring the amount of SN-38 that could be extracted from each of the solid tumors by reverse-phase HPLC. Only slight conversion from CPT-11 to SN-38 was seen from 1 to 24 h in the Capan1 tumor and from 1 to 48 h in the PSN1 tumor, and no SN-38 was detected thereafter. In contrast, SN-38 released from NK012 continued to be detected in both tumors from 1 to 96 h after the injection of NK012 (Fig. 5).

Discussion

Recently, several new formulations categorized as DDS have been approved in the field of oncological treatment, such as Doxil, a polyethylene glycol-liposome incorporating adriamycin,[10,11] and abraxane, a taxol coated with albumin.[12,13] In addition, several clinical trials of drugs based on the DDS concept are now underway.[14–16] Because such formulations possess a longer plasma area under the curve (AUC), liposomal drugs should have sufficient time to exit from tumor blood vessel and accumulate at reasonably high dose levels in the surrounding interstitium.

It has been reported that although polyethylene glycol (PEG) liposomes can be delivered efficiently to a solid tumor, free drug is not transferred sufficiently to cancer cells, particularly those that are distant from the tumor vessels, because the formulations are too large to move through the tumor interstitium.[17] Also, it has been suggested that liposomes are too stable to allow the drug within to be released easily. Therefore, it has been speculated that PEG liposomes may not be so effective against cancers in which the tumor vessel network is irregular and loose because of an abundant collagen-rich matrix. Some examples of such cancers include scirrhous cancer of the stomach and pancreatic cancer. In fact, Doxil is known to be clinically effective against ovarian and breast cancers, both of which are characterized by a high density of tumor microvessels, whereas it is not effective against stomach and pancreatic cancers.[18] Therefore, it is conceivable that some special device is necessary for DDS drugs to exert their antitumor effect sufficiently even against hypovascular tumors such as pancreatic cancer.

In the present study, we characterized the tumor vessel and its interstitium using four kinds of human pancreatic xenografts. The results revealed that the number of tumor blood vessels was inversely related to the amount of collagen within the tumor tissues. Among the four cell lines, Capan1 was the poorest in

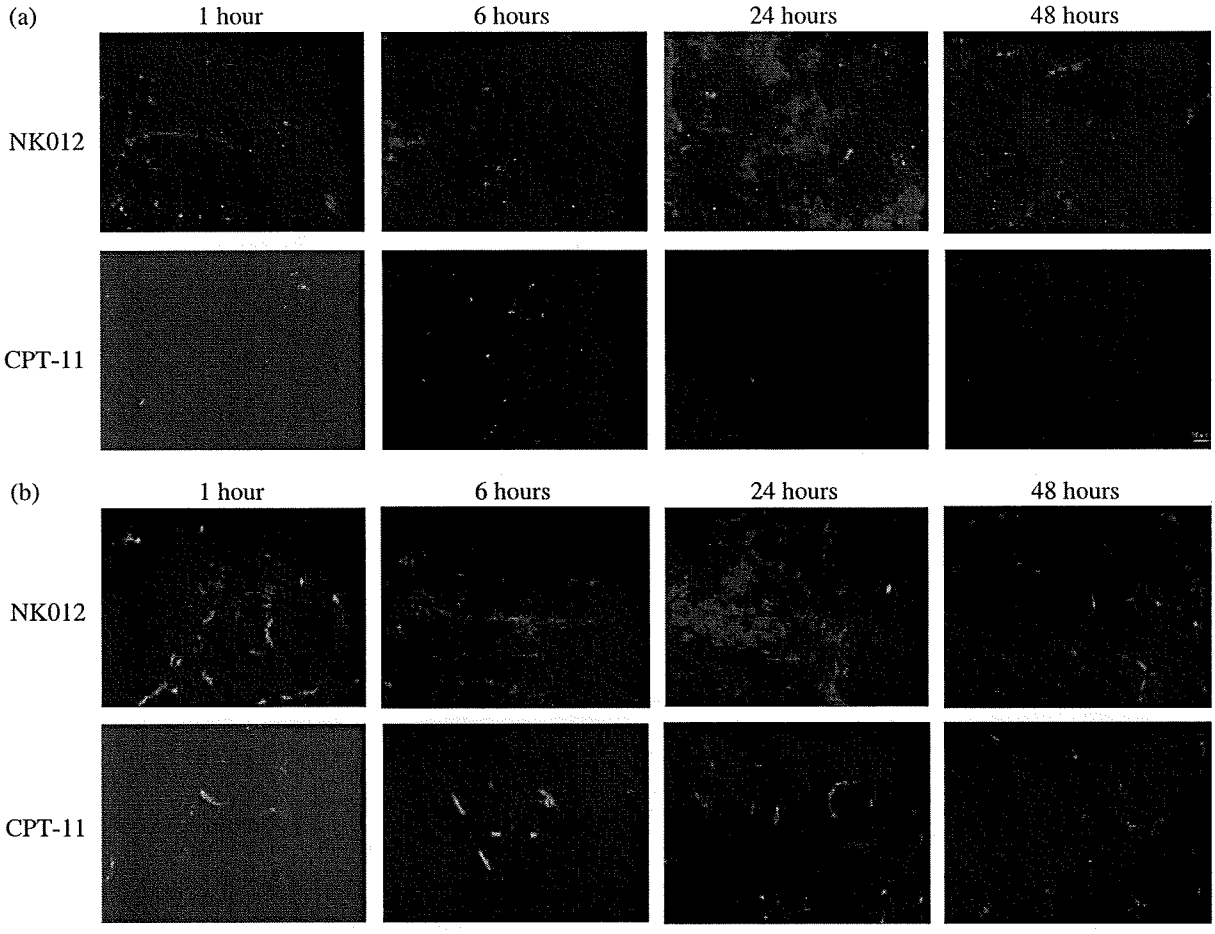

Fig. 4. Distribution of NK012 or CPT-11 in the (a) Capan1 and (b) PSN1 tumor xenografts. Mice bearing Capan1 or PSN1 tumors were injected with NK012 (30 mg/kg/day) or CPT-11 (66.7 mg/kg/day). The tumor tissues were excised at 1, 6, 24, and 48 h after the intravenous injection of NK012 or CPT-11. Each mouse was administered an injection of fluorescein-labeled *Lycopersicon esculentum* lectin just before being killed, for detecting the tumor blood vessels. The frozen sections were examined under a fluorescence microscope at an excitation wavelength of 377 nm and emission wavelength of 447 nm. The same fluorescence conditions can be applied for visualizing NK012 and CPT-11 fluorescence. Free SN-38 can not be detected under these fluorescence conditions.

tumor vasculature and richest in the amount of collagen within the tumor tissue. Conversely, PSN1 was the richest in tumor vasculature and poorest in the amount of collagen. Therefore, it may safely be said that Capan1 xenografts are most like human pancreatic cancer tissue in terms of the amount of interstitial tissue among the four cell lines tested.

We evaluated the *in vitro* cytotoxic effect of CPT-11, SN-38, and NK012 and the *in vivo* antitumor activity of CPT-11 and NK012 against Capan1 tumors as a hypovascular tumor model and PSN1 tumors as a hypervascular tumor model. SN-38 and NK012 exhibited a higher cytotoxic effect against the two cell lines compared with CPT-11. Between SN-38 and NK012, the cytotoxic effect of NK012 was almost similar or a little lower compared with that of SN-38. As CPT-11 itself is a prodrug and is converted to SN-38, an active metabolite of CPT-11, by carboxylesterases, the activity of CPT-11 is dependent on the activity of the enzymes. It is speculated that the efficient sustained release of SN-38 from NK012 allows the formulation to exert a similar cytotoxic effect to that of SN-38. In the *in vivo* experiment, CPT-11 showed significant antitumor activity against both PSN1 tumors as a hypervascular tumor model and Capan1 tumors as a hypovascular tumor model. A slight reduction in tumor size was observed from day 4 to 12 in the case of PSN1 tumors, but not Capan1 tumors. We suggest that the higher antitumor activity seen in PSN1 compared with Capan1 tumors is probably because of the greater accumulation of CPT-11 in the PSN1 xenografts because of the more abundant vasculature. Surprisingly, NK012 could cause complete disappearance of both PSN1 and Capan1 tumor xenografts. Before conducting the experiment, we had anticipated that NK012 might exert stronger antitumor effects against PSN1 compared with Capan1, because such macromolecular drugs can accumulate more efficiently in the PSN1 xenografts because of the richer vasculature. Therefore, we then intensively examined the distribution of NK012 and CPT-11 within the PSN1 or Capan1 xenografts by fluorescence microscopy and HPLC. In the analysis by fluorescence microscopy, NK012 appeared within and around the tumor blood vessels in both the PSN1 and Capan1 xenografts at 1 h after the injection. NK012 began to spread from the blood vessels within the tumor tissue of both xenografts. Fluorescence originating from NK012 increased to a maximum in both of the tumors by 24 h after the injection of NK012. Namely, NK012 was distributed throughout the entire body of both tumors at 24 h after the injection. Furthermore, fluorescence originating from NK012 was clearly and diffusely detected throughout both tumors.

However, fluorescence originating from CPT-11 increased to a maximum at 1 h in both tumors after the injection of CPT-11, indicating that maximum distribution of CPT-11 was achieved

doi: 10.1111/j.1349-7006.2008.00806.x

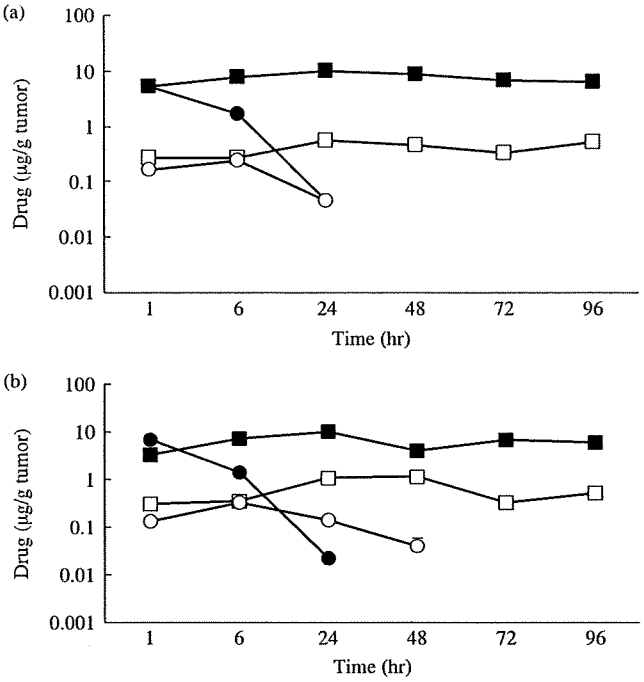

Fig. 5. Tumor distribution of CPT-11, NK012 (or polymer bound SN-38), and free SN-38 after administration of NK012 and CPT-11 to mice bearing (a) Capan1 or (b) PSN1 xenografts. The time profiles of polymer-bound SN-38 (■), free SN-38 released from NK012 (□), CPT-11 (●), and free SN-38 converted from CPT-11 (○) were obtained by high-performance liquid chromatography analysis. The time points examined were 1, 6, 24, 48, 72, and 96 h after the administration of CPT-11 or NK012.

in both tumors within 1 h of the injection. No or very slight fluorescence of CPT-11 was observed in the tumors at 6 h after CPT-11 injection. These observations were confirmed quantitatively by measuring the amount of SN-38 extracted from both tumors by reverse-phase HPLC. Only slight conversion to SN-38 from CPT-11 was seen from 1 to 24 h in the Capan1 tumor and from 1 to 48 h in the PSN1 tumor, and no SN-38 was detected thereafter. SN-38 released from NK012 continued to be detected in both tumors from 1 to 96 h after the injection of NK012. In both CPT-11 and NK012, SN-38 binds to each counter molecule via an ester bond, which confers blue fluorescence on CPT-11 and NK012. Therefore, it is speculated that polymer-bound SN-38 can be distributed throughout the entire body of the tumor, regardless of the amount of interstitial tissue. We are unable to explain clearly how NK012 was distributed well even in hypovascular tumors. However, it is speculated that NK012 can move smoothly within the tumor interstitium because of its relatively small particle size (20 nm) compared with other DDS formulations, and because of its flexibility the formulation can pass through even narrow gaps within the interstitium. Previously, we reported that sustained release of 74% free SN-38 occurred from NK012 under physiological conditions within 48 h.[8] It is also important to remember that the antitumor activity of SN-38 is time dependent.[19] Taking all of these data together, it may be concluded that NK012 can selectively accumulate in pancreatic tumor xenografts, to be distributed effectively throughout the entire body of the tumor, including in hypovascular tumors, and shows sustained release for a prolonged period of time. Consequently, NK012 can exert more significant antitumor activity than CPT-11, which is not an ideal formulation for realizing the time-dependent actions of the drug.

In addition to our present study, there have been several efforts to enhance the accumulation of anticancer agents in tumors to obtain higher antitumor activities of drugs. For example, it has been reported that a transforming growth factor-β inhibitor can enhance tumor vascular permeability to promote accumulation of macromolecules.[20] Conversely, combined use of an antiangiogenic agent, such as an antibody to VEGF, with an anticancer agent could enhance the antitumor activity, probably by lowering the tumor vascular permeability with a consequent decrease in the interstitial fluid pressure so that the anticancer agents may accumulate more easily in the tumor.[21,22] However, much remains to be clarified.

In the present paper, we have shown not only the superiority of the antitumor effect of NK012 compared with that of CPT-11, but also propose that enhanced accumulation, distribution, and retention of DDS within the tumor tissue and the sustained release of anticancer agents from DDS particles are key elements for the treatment of hypovascular tumors. A phase I clinical trial is now underway. Not only the clinical usefulness of NK012, but also the new concept for antitumor actions described in this paper are intended to be verified in the near future through further preclinical and clinical studies.

Acknowledgments

We thank Mrs H. Miyatake and Mrs N. Mie for their technical assistance and Mrs K. Shiina for her secretarial assistance. This work was supported partly by a Grant-in-Aid from the 3rd Term Comprehensive Control Research for Cancer, Ministry of Health, Labor and Welfare (Y. Matsumura) and Scientific Research on Priority Areas from the Ministry of Education, Culture, Sports, Science and Technology (Y. Matsumura).

References

1 Jemal A, Siegel R, Ward E, Murray T, Xu J, Thun MJ. Cancer statistics, 2007. *CA Cancer J Clin* 2007; **57**: 43–66.
2 Burris HA 3rd, Moore MJ, Andersen J *et al.* Improvements in survival and clinical benefit with gemcitabine as first-line therapy for patients with advanced pancreas cancer: a randomized trial. *J Clin Oncol* 1997; **15**: 2403–13.
3 Moore MJ, Goldstein D, Hamm J *et al.* Erlotinib plus gemcitabine compared with gemcitabine alone in patients with advanced pancreatic cancer: a phase III trial of the National Cancer Institute of Canada Clinical Trials Group. *J Clin Oncol* 2007; **25**: 1960–6.
4 Hosoki T. Dynamic CT of pancreatic tumors. *AJR Am J Roentgenol* 1983; **140**: 959–65.
5 Sofuni A, Iijima H, Moriyasu F *et al.* Differential diagnosis of pancreatic tumors using ultrasound contrast imaging. *J Gastroenterol* 2005; **40**: 518–25.
6 Matsumura Y, Maeda H. A new concept for macromolecular therapeutics in cancer chemotherapy: mechanism of tumoritropic accumulation of proteins and the antitumor agent smancs. *Cancer Res* 1986; **46**: 6387–92.
7 Muggia FM. Doxorubicin-polymer conjugates: further demonstration of the concept of enhanced permeability and retention. *Clin Cancer Res* 1999; **5**: 7–8.
8 Koizumi F, Kitagawa M, Negishi T *et al.* Novel SN-38-incorporating polymeric micelles, NK012, eradicate vascular endothelial growth factor-secreting bulky tumors. *Cancer Res* 2006; **66**: 10 048–56.
9 Kawato Y, Furuta T, Aonuma M, Yasuoka M, Yokokura T, Matsumoto K. Antitumor activity of a camptothecin derivative, CPT-11, against human tumor xenografts in nude mice. *Cancer Chemother Pharmacol* 1991; **28**: 192–8.
10 Muggia FM. Liposomal encapsulated anthracyclines: new therapeutic horizons. *Curr Oncol Rep* 2001; **3**: 156–62.
11 Ferrari M. Cancer nanotechnology: opportunities and challenges. *Nat Rev Cancer* 2005; **5**: 161–71.
12 Green MR, Manikhas GM, Orlov S *et al.* Abraxane, a novel Cremophor-free, albumin-bound particle form of paclitaxel for the treatment of advanced non-small-cell lung cancer. *Ann Oncol* 2006; **17**: 1263–8.
13 Gradishar WJ, Tjulandin S, Davidson N *et al.* Phase III trial of nanoparticle albumin-bound paclitaxel compared with polyethylated castor oil-based paclitaxel in women with breast cancer. *J Clin Oncol* 2005; **23**: 7794–803.
14 Matsumura Y, Hamaguchi T, Ura T *et al.* Phase I clinical trial and pharmacokinetic evaluation of NK911, a micelle-encapsulated doxorubicin. *Br J Cancer* 2004; **91**: 1775–81.

15 Hamaguchi T, Matsumura Y, Suzuki M *et al.* NK105, a paclitaxel-incorporating micellar nanoparticle formulation, can extend *in vivo* antitumour activity and reduce the neurotoxicity of paclitaxel. *Br J Cancer* 2005; **92**: 1240–6.
16 Uchino H, Matsumura Y, Negishi T *et al.* Cisplatin-incorporating polymeric micelles (NC-6004) can reduce nephrotoxicity and neurotoxicity of cisplatin in rats. *Br J Cancer* 2005; **93**: 678–87.
17 Unezaki S, Maruyama K, Hosoda J *et al.* Direct measurement of the extravasation of polyethylene glycol-coated liposomes into solid tumour tissue by *in vivo* fluorescence microscopy. *Int J Pharmacol* 1996; **144**: 11–17.
18 Tsukioka Y, Matsumura Y, Hamaguchi T, Koike H, Moriyasu F, Kakizoe T. Pharmaceutical and biomedical differences between micellar doxorubicin (NK911) and liposomal doxorubicin (Doxil). *Jpn J Cancer Res* 2002; **93**: 1145–53.
19 Kawato Y, Aonuma M, Hirota Y, Kuga H, Sato K. Intracellular roles of SN-38, a metabolite of the camptothecin derivative CPT-11, in the antitumor effect of CPT-11. *Cancer Res* 1991; **51**: 4187–91.
20 Kano MR, Bae Y, Iwata C *et al.* Improvement of cancer-targeting therapy, using nanocarriers for intractable solid tumors by inhibition of TGF-β signaling. *Proc Natl Acad Sci USA* 2007; **104**: 3460–5.
21 Jain RK. Normalizing tumor vasculature with anti-angiogenic therapy: a new paradigm for combination therapy. *Nat Med* 2001; **7**: 987–9.
22 Jain RK. Normalization of tumor vasculature: an emerging concept in antiangiogenic therapy. *Science* 2005; **307**: 58–62.

doi: 10.1111/j.1349-7006.2008.00806.x

J. Radiat. Res., 49, 29–40 (2008) Regular Paper

Gene Expression Profiles in Mouse Liver Cells after Exposure to Different Types of Radiation

Mehryar Habibi ROUDKENAR[1,2], Li LI[1], Taisuke BABA[1], Yoshikazu KUWAHARA[1], Hironobu NAKAGAWA[1], Lu WANG[1], Satoshi KASAOKA[3], Yasuhito OHKUBO[4], Koji ONO[5] and Manabu FUKUMOTO[1]*

Gene expression/Microarray/Mouse liver/Radiation quality/Endothelial cell/Kupffer cell.

The liver is one of the target organs of radiation-induced cancers by internal exposures. In order to elucidate radiation-induced liver cancers including Thorotrast, we present a new approach to investigate *in vivo* effects of internal exposure to α-particles. Adopting boron neutron capture, we separately irradiated Kupffer cells and endothelial cells in mouse liver *in vivo* and analyzed the changes in gene transcriptions by an oligonucleotide microarray. Differential expression was defined as more than 3-fold for up-regulation and less than 1/3 for under-regulation, compared with non-irradiated controls. Of 6,050 genes examined, 68 showed differential expression compared with non-irradiated mice. Real-time polymerase chain reaction validated the results of the microarray analysis. Exposure to α-particles and γ-rays produced different patterns of altered gene expression. Gene expression profiles revealed that the liver was in an inflammatory state characterized by up-regulation of positive acute phase protein genes, irrespective of the target cells exposed to radiation. In comparison with chemical and biological hepatotoxicants, inductions of Metallothionein 1 and Hemopexin, and suppressions of cytochrome P450s are characteristic of radiation exposure. Anti-inflammatory treatment could be helpful for the prevention and protection of radiation-induced hepatic injury.

INTRODUCTION

The biological effects of exposure to high linear energy transfer (LET) radiation have a particular relevance to radiation protection and risk assessment. Although internal exposure to high LET radiation is of a major concern, it is characterized by the existence of target organs and the difficulty of dose estimation. Thorotrast, a colloidal suspension of radioactive $^{232}ThO_2$ that naturally emits α-particles, was used as a radiographic contrast agent in the 1930s–1950s. More than half of intravasculary injected Thorotrast deposited in the liver caused liver cancers decades after the injection because of its life-long deposition and exposure to α-particles. Our histological examination of the liver from 144 cases of Thorotrast patients revealed intrahepatic cholangiocellular carcinoma (ICC, 25.7%), angiosarcoma (AS, 20.8%), hepatocellular carcinoma (HCC, 14.6%) and combined tumors (2.1%). Considering that Japan is an endemic area of hepatitis virus B and C, and that HCC comprises more than 80% of liver cancers, ICC and AS may be considered to be characteristic of Thorotrast-induced liver tumors. Our previous study showed that injected Thorotrast is phagocytosed by macrophages and radioactive Thorium is always migrating within the affected livers via Thorotrast-laden macrophages. These suggest that the liver is evenly exposed to α-particles at the organ level despite the short range of α-particles.[1)] Internal deposition of plutonium also causes chronic exposure to high levels of α-particles with increased risk of liver cancers including AS.[2)] Neither the deposited amount of Thorium nor the incubation period from injection to tumor induction is significantly different between cases with ICC and AS (manuscript in preparation). Consequently we thought that cell-to-cell interaction between irradiated macrophages and/or epithelial cells and parenchymal cells of the liver is involved in the development of ICC while direct irradiation of endothelial cells of the

*Corresponding author: Phone: +81-22-717-8507,
Fax: +81-22-717-8512,
E-mail: fukumoto@idac.tohoku.ac.jp
[1]Department of Pathology, Institute of Development, Aging and Cancer, Tohoku University, Sendai 980-8575, Japan; [2]Research Center, Iranian Blood Transfusion Organization Tehran, Iran; [3]Faculty of Pharmaceutical Sciences, Hiroshima International University, Hiroshima 737-0112, Japan; [4]Department of Radiopharmacology, Tohoku Pharmaceutical University, Sendai 981-8558, Japan; and [5]Radiation Oncology Research Laboratory, Research Reactor Institute, Kyoto University, Osaka 590-0494, Japan.
doi:10.1269/jrr.07078

sinusoid is the principal contributor to the development of AS. A few studies also have been shown that exposure to α-particles induces liver tumors in mouse and other rodents.[3,4]

Thermal neutrons cause the boron atom to split into an α-particle and a lithium nucleus via the boron neutron capture reaction (BNC). Both of these particles have a very short range (about one cellular diameter) and cause significant damage to the cell in which boron atoms are located. BNC therapy (BNCT) adopts this cytotoxic effect by selective delivery of boron-10 (^{10}B) to tumor cells: the short range nature of the effects of BNC minimizes the damage to adjacent normal cells. A large amount of ^{10}B compound can be administered in a liposome-incorporated form, which is then phagocytosed by macrophages. Conjugation of the liposome with polyethylene glycol (PEG) is known to increase blood levels of ^{10}B compounds and reduced uptake by macrophages.[5] Recent radiological studies focus on the molecular mechanisms underlying transcriptional responses of mammalian cells to ionizing radiation. It is now apparent that the cellular reactions to ionizing radiation are complex and involve the activation of secondary messenger pathways and increased transcription of immediate early response genes.[6]

These observations prompted us to adopt BNC to investigate *in vivo* effects of internal radiation exposure to α-particles. In this study, we prepared the ^{10}B-liposome treatment and the ^{10}B PEG-liposome treatment to expose Kupffer cells and endothelial cells to α-particles respectively, and analyzed the changes of gene expression using a microarray containing probes for 6,050 genes. As well as elucidation of the biological relevance of radiation, the present study also

Table 1. Primer sets for RT-PCR

Symbol	GenBank		Sequence	Size(bp)
AK3	AK005194	forward reverse	5'-GTG TGT TGG CCA AGA CTT TC-3' 5'-ATG TAT CCA GCG AGC AGT AAG-3'	236
Atp5b	AK010314	forward reverse	5'-GCA CAA TGC AGG AAA GGA TCA C-3' 5'-ACG TCA TAA TGC TCA TTG CCA AC-3'	241
ATP5c1	AK007063	forward reverse	5'-CGC CCC ATG GCA ACT CTG AAA G-3' 5'-GCC AAA GAA CCT GTC CCA TAC A-3'	160
Brap	AK013885	forward reverse	5'-AAA GGG CTG AAG TGC TGA ATC-3' 5'-TCT GGC GTT TGA CAG TAT CGG C-3'	211
Car3	AK003671	forward reverse	5'-CTT GAT GCC CTG GAC AAA AT-3' 5'-AGC TCA CAG TCA TGG GCT CT-3'	180
Egfr	AK004944	forward reverse	5'-TGA GCA ACA TGT CAA TGG ACT TAC-3' 5'-GCA TGT GGC CTC ATC TTG GAA C-3'	263
Galnt3	AK019995	forward reverse	5'-CAC TAT TTA CCC GGA AGC GTA TG-3' 5'-GTG GCA CGT GTA CAG AAT CAA TG-3'	139
Gsta3	AK014076	forward reverse	5'-TGA CCT GGC AAG GTT ACG AAG TG-3' 5'-CAT TAT CTC CAG ATC CGC CAC TC-3'	199
Hpxn	BB610094	forward reverse	5'-ATC TCA GCG AG GTG GAA GAA TC-3' 5'-CCT TCA CTC TGG CAC TCT CCA C-3'	215
Lcn2	AK002932	forward reverse	5'-CCA GTT CGC CAT GGT ATT TTT C-3' 5'-CAC ACT CAC CAC CCA TTC AGT T-3'	206
Mt1	AK018727	forward reverse	5'-ACC TCC TTG CAA GAA GAG CTG CT-3' 5'-GCT GGG TTG GTC CGA TAC TAT T-3'	160
Mt2	AK002567	forward reverse	5'-GGG TCC CCA CAT CTG TG TAA-3' 5'-CAA CGG CTT TTA TTG TCA GTT AC-3'	115
β-actin		forward reverse	5'-TTC TAC AAT GAG CTG CGT GTG G-3' 5'-GTG TTG GAA GGT CTC AAA CAT GAT-3'	110

contributes to the understanding of general idea of potential target molecules for cancer therapy.

MATERIALS AND METHODS

Mice and radiation

Male C3H/Hex mice (6 weeks old) were exposed to whole-body irradiation. For irradiation of mice by α-particles, specifically to macrophages and endothelial cells, ^{10}B-liposomes and polyethylene glycol (PEG)-^{10}B-liposomes were respectively administered. There were two mice analyzed by microarray, independently treated, and five mice by real time PCR. Mice used for these 2 assays were from 2 different courses of experiments. The ^{10}B compound sodium mercaptoundecahydrododecaborate (BSH) was used.[7] Each compound was suspended in physiological saline at a concentration of 4,000 ppm and 100 μl of ^{10}B-liposome solution and 300 μl of PEG-^{10}B-liposome solution were injected via the tail vein. Four hours (hrs) after the administration, the mice were exposed to neutron radiation at the Research Reactor Institute, Kyoto University (RRIKU). Before the irradiation experiments for gene expression, the neutron fluence was monitored by radioactivation of gold foils in the front and back of the mouse container. The average fluence of the thermal neutron source was 2.1×10^{12} n/cm^2 and the average flux was 2.3×10^9 n/cm^2/s at 5 MW. The boron concentration of the liver was measured by γ-ray spectrometry using a thermal neutron guide. We determined the exposure period at the calculated dose of 8.5 Gy at an organ level. For control irradiation, the mice were exposed to the neutron source for the same period as the BNC group. The contribution of neutrons and γ-rays to the total exposure was 4.2 cGy and 33 cGy, respectively. As a control for the quality of radiation, the mice were exposed to γ-rays at a dose of 8.5 Gy (0.34 Gy/min) with a ^{60}Co γ-ray source. Twenty hrs after irradiation, the mice were sacrificed by cervical dislocation. The dissected liver was immediately frozen and stored at –80°C until use. Animal experiments were approved by the Ethical Committee of the Institute of Development, Aging and Cancer, Tohoku University and were performed in accordance with institutional guidelines.

Oligonucletide microarrays

In accordance with 'Functional Annotation of Mouse' for the RIKEN full-length cDNA clone (http://fantom2.gsc.riken.go.jp/) and GenBank (http://www.ncbi.nih.gov/Genbank), 6,050 mouse genes were chosen for microarray analysis. These consisted of genes associated with signal transduction (766), cancer (506), autoimmune/inflammatory disease (455), cytokine/inflammatory response (267), stem cell

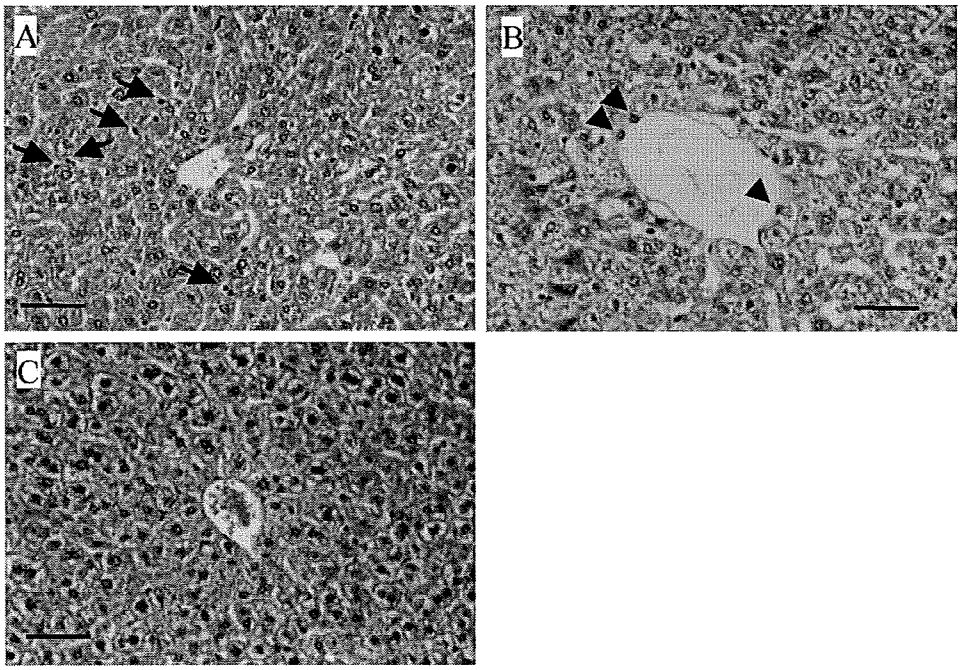

Fig. 1. Histological findings of the mouse liver following irradiation of Kupffer or endothelial cells. A: Compared with non-irradiated control, mice injected with ^{10}B-liposome solution showed a slight increase of the number and the size of Kupffer cells (arrows), indicating Kupffer cells were mainly irradiated (Kupffer exposure). B: Endothelial cells (arrow heads) were swollen in irradiated liver. The dilatation of sinusoids was noticed in mice injected with PEG-^{10}B-liposome, indicating sinusoidal endothelial cells were mainly insulted (Endothelial exposure). C: Non-irradiated control. Scale Bar: 50 μm.

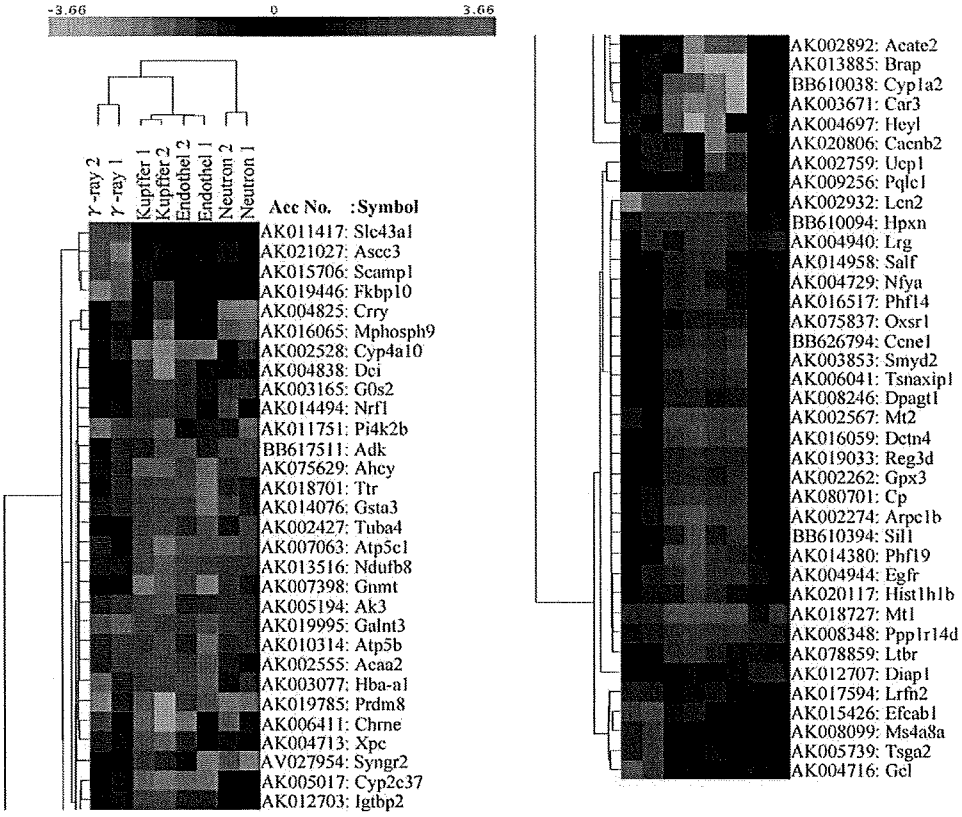

Fig. 2. Cluster analysis of individual mice according to the profile of gene expression examined. Mice from the same exposure group was the closest and the neutron exposure group was the most different from other groups.

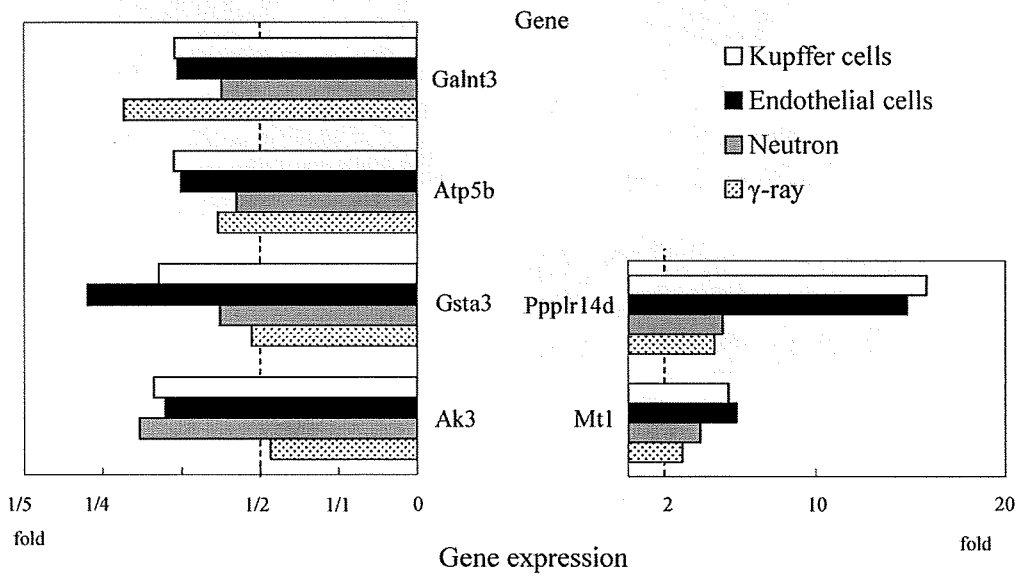

Fig. 3. Genes which are commonly over-expressed more than 2-fold or under-expressed less than a half following irradiation compared to control gene expression levels. Ak3: Adenylate kinase 3α, Gsta3: Glutathione S-transferase 3α, Atp5b: ATP synthase β subunit, Galnt3: UDP-N-acetyl-α-D-galactosamine-polypeptide, Mtl: Metallothionein 1, Ppp1r14d: Protein phosphatase 1, regulatory (inhibitor) subunit 14D.

(261), apoptosis (260), cardiovascular disease (240), neuroscience (197), toxicology/pharmacology (184), extracellular matrix/adhesion molecules (105), diabetes/obesity (105), developmental/regenerative disorder (102), cell cycle (99), and others (2,503).

After total RNA was extracted from the liver using TRIZOL reagent (Invitrogen Corp., Carlsbad, CA), Poly-A RNA was separated using dT(25)-coupled magnetic beads (Dynal Biotech, Oslo, Norway). Individual mice were evaluated for the change in gene expression against pooled liver RNA

Table 2-A. Up and down-regulated genes in all the irradiated groups

	Gene	Symbol	GenBank	Function
Up	Metallothionein 1	Mt1	AK018727	Metal binding
	Protein phosphatase 1, regulatory (inhibitor) subunit 14D	Ppp1r14d	AK008348	Protein phosphatase inhibitor
Down	Adenylate kinase 3α	Ak3	AK005194	Adenine metaboilsm
	Glutathione S-transferase α3	Gsta3	AK014076	Detoxication
	ATP synthase β subunit	Atp5b	AK010314	ATP synthesis
	UDP-N-acetyl-α-D-galactosamine-polypeptide	Galnt3	AK019995	Secretion

Table 2-B. Commonly up and down-regulated genes by Kupffer cell specific and endothelial cell specific exposures to α-particles

	Gene	Symbol	GenBank	Function
Up	Lipocalin 2	Lcn2	AK002932	Anti-apoptosis
	Metallothionein 2	Mt2	AK002567	Metal binding
	Actin related protein 2/3 complex, subunit 1B	Arpc1b	AK002274	Cytoskeleton, protein trafficking
	Dynactin 4	Dctn4	AK016059	Cytoskeleton, protein trafficking
	PHD finger protein 19	Phf19	AK014380	Chromatin regulation
	Epidermal growth factor receptor	Egfr	AK004944	Cell growth
	SET and MYND domain containing 2	Smyd2	AK003853	Transcription
	Endoplasmic reticulum chaperone SIL1 homolog	Sil1-pening	BB610394	Molecular chaperon
	Hemopexin	Hpxn	BB610094	Metal transporter, antioxidant
	Ceruloplasmin	Cp	AK080701	Metal transporter
	Cyclin E1	Ccne1	BB626794	Cell cycle
	Translin-associated factor X (Tsnax) interacting protein 1	Tsnaxip1	AK006041	Cell cycle
	Regenerating islet-derived δ	Reg3d	AK019033	Cell growth
	Glutathione peroxidase 3	Gpx3	AK002262	Antioxidant
Down	PR domain containing 8	Prdm8	AK019785	Chromatin regulation
	CYP4A10	Cyp4a10	AK002528	Metabolism
	S-adenosylhomocysteine hydrolase	Ahcy	AK075629	Adenosine metabolism
	Glycine N-methyltransferase	Gnmt	AK007398	Methylation
	CYP2C37	Cyp2c37	AK005017	Metabolism
	Carbonic anhydrase 3	Car3	AK003671	Antioxidant
	ATP synthase γ subunit	Atp5c1	AK007063	ATP synthesis
	NADH dehydrogenase (ubiquinone) 1β subcomplex 8	Ndufb8	AK013516	Electron transport
	Transthyretin	Ttr	AK018701	Negative acute phase protein
	CYP1A2	Cyp1a2	BB610038	Metabolism

Table 2-C. Up and down-regulated genes by Kupffer cell specific exposure to α-particles

	Gene	Symbol	GenBank	Function
Up	Lymphotoxin B receptor	Ltbr	AK078859	Immunity
	Histone 1, H1b	Hist1h1b	AK020117	Chromosome organization
	PHD finger protein 14	Phf14	AK016517	Chromatin regulation
	Stoned B/TFIIA- α/β -like factor	Salf	AK014958	Transcription factor, membrane traficking
	Nuclear transcription factor-Y α	Nfya	AK004729	Transcription factor
	UDP-GlcNAc:dolichyl-phosphate N-acetylglucosamine photransferase 1	Dpagt1	AK008246	Protein glycosylation
Down	Nicotinic cholinergic receptor, ε polypeptide	Chrne	AK006411	Neurotransmitter/receptor
	Hairy/enhancer-of-split related with YRPW motif	Heyl	AK004697	Transcriptioin repressor
	3,2 trans-enoyl-CoA isomerase	Dci	AK004838	b-Oxidation of unsaturated fatty acids
	Xeroderma pigmentosum, complementation group C	Xpc	AK004713	DNA repair
	G0/G1 switch gene 2	G0s2	AK003165	G0/G1 transition
	Tubulin, α 4	Tuba4	AK002427	Cytoskeleton
	Nuclear respiratory factor 1	Nrf1	AK014494	Transcription factor
	Acetyl-CoA-acyl transferase 2	Acaa2	AK002555	Fatty acid oxidation
	Insulin-like growth factor binding protein 2	Igfbp2	AK012703	Cell growth regulation

Table 2-D. Up and down-regulated genes by endothel specific exposure to α-particles

	Gene	Symbol	GenBank	Function
Up	Uncoupling protein 1	Ucp1	AK002759	Heat production
	Leucine-rich α-2-glycoprotein1	Lrg1	AK004940	Acute phase protein
	PQ loop repeat containing 1	Pqlc1	AK009256	Electron carrier
	Oxidative-stress responsive 1	Oxsr1	AK075837	Cytoskeleton
Down	BRCA1 associated protein	Brap	AK013885	DNA repair
	Voltage-dependent Ca channel (β2)	Cacnb2	AK020806	Ion channel
	Hemoglobin α adult chain 1	Hba-a1	AK003077	Oxygen delivery
	Acyl-CoA thioesterase 2	Acate2	AK002892	Signal trans., protein traffick

Table 2-E. Up and down-regulated genes by γ-ray exposure

	Gene	Symbol	GenBank	Function
Up	EF hand calcium binding domain 1	Efcab1	AK015426	Ca binding
	Germ cell-less homolog	Gcl	AK004716	Differentiation
	Testis specific gene A2	Tsga2	AK005739	Testis specific
	Membrane-spanning 4-domains, subfamily A, member 8A	Ms4a8a	AK008099	Transporter
	Leucine rich repeat and fibronectin type III domain containing 2	Lrfn2	AK017594	Cell adhesion signal trans.
Down	FK506 binding protein 10	Fkbp10	AK019446	Immunosuppression
	Activating signal cointegrator 1 complex subunit	Ascc3	AK021027	Transcription coactivator
	Secretory carrier membrane protein 1	Scamp1	AK015706	Endocytosis
	Solute carrier family 43, member 1	Slc43a1	AK011417	Transporter

Table 2-F. Up and down-regulated genes by neutron exposure

	Gene	Symbol	GenBank	Function
Up	Diaphanous homolog 1	Diap1	AK012707	Cytoskeleton
Down	Complement receptor related protein	Crry	AK004825	Immunity
	Synaptogyrin 2	Syngr2	AV027954	Synaptic transmission
	Phosphatidylinositol 4-kinase type 2 β	Pi4k2b	AK011751	Inositol lipid biosyhthesis
	M-phase phosphoprotein 9	Mphosph9	AK016065	Cell cycle
	Adenosine kinase	Adk	BB617511	Signal transduction

from the five control non-irradiated mice. Complementary DNA (cDNA) probes were generated starting with 1 μg of polyA RNA using a CyScribe First-Strand cDNA Labelling kit (Amersham Biosciences Corp., Piscataway, NJ). cDNA from irradiated mice was labeled with Cy5 and that from control mice was labeled with Cy3. Pre-hybridization and hybridization were carried out on UltraGAPS coated slides in accordance with the manufacturer's manual (Corning, NY). The image was captured in a GenePix 4000B (Axon Instruments, Inc. CA). The quantification of gene expression arrays was performed by Array Vision software (Imaging Research Inc., Ontario, Canada). Cluster analysis of gene expression was performed by the War method.[8] The experiments were carried out in independent duplicates.

Real-time PCR

In order to validate the results from the microarray analysis we selected 12 genes (Table 1) and compared their gene expression as measured by microarray analysis and real-time PCR. DNaseI treated 500 ng of total RNA was used for the synthesis of cDNA using superscript First-Strand Synthesis System (Invitrogen, Carlsbad, CA). cDNA corresponding to 10 ng of total RNA was amplified using Real-time PCR for the determination of gene expression using QuantiTect SYBR Green PCR Master Mix (QIAGEN K.K., Tokyo, Japan) in an iCycler (BIO-RAD, Hercules, CA). For the normalization of gene expression, a set of primers for β-actin was used.

RESULTS

Compared with non-irradiated controls, mice injected with ^{10}B-liposome solution showed a slight increase in the number and the size of Kupffer cells, indicating that Kupffer cells were irradiated (Kupffer exposure, Fig. 1A). The dilatation of sinusoids was noticed in mice injected with PEG-^{10}B-liposome, indicating sinusoidal endothelial cells were irradiated (Endothelial exposure, Fig. 1B). Liver tissues from mice exposed to γ-rays and neutrons revealed no remarkable histological changes (data not shown). In all cases, parenchymal hepatocytes did not show noticeable changes (Fig. 1).

Table 3. Comparison of gene expressioin levels between microarray and real-time PCR

Symbol	GenBank	endothelial			Kupffer			neutron			gamma		
		Real time-PCR	Micro-Array		Real time-PCR	Micro-Array		Real time-PCR	Micro-Array		Real time-PCR	Micro-Array	
		mean ± S.D.	Mouse 1	Mouse 2	mean ± S.D.	Mouse 1	Mouse 2	mean ± S.D.	Mouse 1	Mouse 2	mean ± S.D.	Mouse 1	Mouse 2
AK3	AK005194	0.66 ± 0.29	0.40	0.45	0.68 ± 0.10	0.29	0.27	0.84 ± 0.28	0.42	0.40	0.95 ± 0.33	0.38	0.48
Atp5b	AK010314	0.52 ± 0.06	0.22	0.44	0.72 ± 0.28	0.35	0.30	0.71 ± 0.17	0.43	0.44	0.90 ± 0.19	0.34	0.45
ATP5c1	AK007063	0.64 ± 0.06	0.27	0.26	0.68 ± 0.07	0.28	0.15	0.83 ± 0.29	0.33	0.28	1.47 ± 0.53	0.91	0.52
Brap	AK013885	0.69 ± 0.14	0.04	0.06	0.89 ± 0.32	0.94	0.13	1.23 ± 0.54	1.66	1.11	2.03 ± 0.71	0.62	0.97
Car3	AK003671	0.07 ± 0.053	0.04	0.20	0.14 ± 0.03	0.26	0.17	0.85 ± 0.27	1.14	1.09	0.53 ± 0.26	0.53	0.74
Egfr	AK004944	1.65 ± 0.84	5.41	4.90	3.39 ± 1.67	5.22	9.07	1.12 ± 0.69	1.68	2.81	1.93 ± 0.81	3.61	1.71
Galnt3	AK019995	0.19 ± 0.05	0.29	0.37	0.39 ± 0.20	0.30	0.34	0.68 ± 0.17	0.43	0.38	0.47 ± 0.06	0.24	0.30
Gsta3	AK014076	0.58 ± 0.14	0.18	0.30	0.85 ± 0.22	0.31	0.30	1.10 ± 0.21	0.46	0.34	0.67 ± 0.10	0.41	0.54
Hpxn	BB610094	36.53 ± 20.07	4.49	6.94	40.33 ± 17.23	6.42	6.38	2.56 ± 1.05	0.61	0.82	8.38 ± 5.3258	6.12	2.90
Lcn2	AK002932	1909.50 ± 558.5	94.79	95.38	1558.30 ± 133.6	34.90	62.41	1.94 ± 1.15	0.79	1.38	6.34 ± 5.20	128.21	–
Mt1	AK018727	24.22 ± 9.13	13.14	16.51	29.51 ± 8.88	15.35	16.38	1.67 ± 0.81	7.20	2.92	15.59 ± 10.66	5.12	4.11
Mt2	AK002567	38.46 ± 25.77	6.47	8.78	42.33 ± 7.71	12.84	19.36	2.57 ± 1.65	2.00	1.37	10.22 ± 7.43	1.99	3.32

Cluster analysis of the microarray results revealed that 2 mice from the same exposure group were the closest, indicating that all the experimental data in this study are reliable (Fig. 2). In this study, only the genes whose over-expression or under-expression compared with non-irradiated control levels which were consistently observed in 2 different mice with the same exposure levels were analyzed. In total, 161 genes were over-expressed by more than 2-fold and 32 genes

Table 4. Comparison of gene expression profiles between radiation exposures and hepatotoxicants

Gene	Symbol	GeneBank	Kupffer cells		Endothel		Neutrons		γ-rays		McMillian *et al.* (rat)	
			Mouse 1	Mouse 2	Mouse 1	Mouse 2	Mouse 1	Mouse 2	Mouse 1	Mouse 2	hepatotoxicants	PPA[a]
Macrophage activation/acute phase response												
Cytochrome P450, family 1, subfamily a, polypeptide 2	Cyp1a2	BB610038	0.32	0.30	0.07	0.15	1.47	1.07	0.63	0.89	0.51	
CYP2C37	Cyp2c37	AK005017	0.23	0.20	0.21	0.23	1.35	1.36	0.60	1.11	0.63	
Fatty acid binding protein 5, epidermal	Fabp5	AK011551	2.85	1.64	1.28	1.76	1.17	1.46	0.71	0.45	2.75	
G-6-phosphatase, transport protein 1	G6pt1	AK003620	0.45	0.43	0.54	0.58	0.70	0.55	0.87	1.39	0.51	0.46
Hemopexin	Hpxn	BB610094	6.41	6.38	4.49	6.94	0.61	0.82	6.12	2.90	1.57	
Insulin-like growth factor binding protein, acid labile subunit	Igfals	AK004926	–	–	–	–	0.32	0.64	1.18	0.52	0.41	
Latent TGF-β binding protein 1	Ltbp1	AK020449	0.41	0.01	0.73	0.08	1.05	0.25	–	0.42	1.06	0.84
Metallothionein 1	Mt1	AK018727	15.35	16.38	13.14	16.51	7.20	2.92	5.12	4.11	1.44	0.23
Pyruvate kinase, muscle	Pkm2	AK002341	1.10	1.23	1.19	1.48	1.00	1.31	1.26	–	2.41	
Retinol binding protein 4, plasma	Rbp4	AK004839	0.32	0.34	0.24	0.40	0.63	0.58	0.61	0.73	0.66	
Superoxide dismutase 2	Sod2	AK002534	1.73	1.77	2.34	1.45	0.76	0.46	1.09	0.96	2.69	
Peroxisome proliferator												
Acetyl-CoA dehydrogenase, medium chain	Acadm	AK008149	0.62	–	0.81	0.87	0.76	0.88	0.52	0.50	0.47	
Brain acyl-CoA hydrolase	Bach	AK010646	1.23	1.25	1.26	1.45	1.06	1.26	0.88	1.02	0.82	2.00
3-hydroxybutyrate dehydrogenase	Bdh	AK009575	0.59	0.66	0.67	0.83	0.76	0.57	0.75	0.54	0.38	
CD36 antigen	Cd36	AK004192	1.20	1.09	1.17	1.15	0.93	1.30	1.10	0.69	1.01	2.87
Dodecenoyl-CoA delta isomerase	Dci	AK004838	0.30	0.10	0.55	0.32	0.54	0.65	0.89	1.10	0.37	1.73
2,4-dienoyl CoA reductase 1	Decr1	AK004725	1.22	1.10	1.11	1.10	1.14	1.22	1.00	0.95	0.45	
Epoxide hydrolase 2	Ephx2	AK002415	0.54	0.55	0.62	0.50	0.99	0.89	0.82	0.75	0.28	
Fatty acid CoA ligase, long chain 2	Facl2	AK004897	0.39	0.32	0.37	0.38	0.68	0.76	0.60	0.73	0.34	
3-hydroxy-3-methylglutaryl-CoA synthase 2	Hmgcs2	AK004865	0.46	0.38	0.48	0.34	1.01	1.21	0.69	1.40	0.44	
ER stress/chaperone protein /HSP												
Annexin A2	Anxa2	AK012563	0.75	1.26	1.45	1.38	1.14	0.93	1.66	–	2.36	
Calreticulin	Calr	AK075605	1.58	1.57	1.35	1.88	0.62	1.21	1.79	1.13	2.28	0.65
Protein disulfide isomerase-related	Pdir	AK012415	1.38	1.35	1.18	0.60	0.94	1.15	0.88	0.58	2.14	0.62
Metabolism												
S-adenosylhomocysteine hydrolase	Ahcy	AK075629	0.21	0.18	0.14	0.26	0.30	0.35	0.42	0.64	0.41	
Betaine-homocysteine methyltransferase	Bhmt	AK016283	1.49	1.70	1.27	1.52	1.20	1.39	1.58	1.99	0.24	
Sulfotransferase family 1A, phenol-preferring, member 1	Sult1a1	AK002700	0.41	0.43	0.35	0.49	0.57	0.59	0.92	0.99	0.43	
Other functions												
G0/G1 switch gene 2	G0s2	AK003165	0.30	0.27	0.48	0.34	0.38	0.36	1.35	2.07	0.60	
Kininogen	Kng	AK005547	1.71	2.65	2.55	2.70	1.37	1.21	1.61	1.04	1.16	0.68
Solute carrier family 34 , member 2	Slc34a2	AK004832	0.45	0.23	0.81	1.78	0.74	1.18	1.24	1.37	1.06	1.59

Light gray background: Under-expressed genes; Black: Over -expressed genes
[a]: Peroxisome proliferator agonist

were over-expressed by more than 3-fold by exposure to either type of radiation. Of the under-expressed genes, 194 showed an expression level of less than 1/2, compared to the control levels and 36 genes showed less than 1/3 compared to the control levels. Approximately the same number of genes showed over-expression of between 2- and 3-fold or under-expression of between a half and a third. Therefore, we defined a gene to be up-regulated when the mean value of its expression levels in exposed mice showed more than a 3-fold over-expression, and down-regulated if its expression level was less than 1/3 compared with non-irradiated mice.

In terms of gene expression profile, Kupffer and endothelial exposures were the most similar to and the neutron exposure group was the most different from other groups (Fig. 2). For commonly up- and down-regulated genes in all the exposure groups, we picked up genes with a level of over-expression of more than 2-fold and under-expression of less than a half among all the radiation groups. Commonly up-regulated genes were metallothionein 1 (Mt1) and protein phosphatase 1, regulatory (inhibitory) subunit 14D (Ppp1r14d). Commonly down-regulated genes were adenylate kinase 3α (Ak3), glutathione S-transferase 3α (Gsta3), ATP (Adenosine triphosphate) synthase β subunit (Atp5b) and UDP (uridine diphosphate)-N-acetyl-α-D-galactosamine-polypeptide (Galnt3) (Fig. 3 and Table 2-A). Commonly up- and down-regulated genes between Kupffer cell irradiation and endothelial cell irradiation are shown in Table 2-B. There were 14 up-regulated genes: 5 associated with cell-cycle regulation, 3 associated with intracellular transportation, 3 that code for metal binding proteins and 3 others. There were 10 down-regulated genes, composed of 3 cytochrome P450 (CYP) genes, 3 associated with ATP synthesis and 4 others. For the genes whose changes in expression were specific to irradiated Kupffer cells, molecules associated with transcription including histone H1 were 3 of 6 up-regulated genes. Of the 9 down-regulated genes, 2 each were respectively associated with cell cycle, transcription and fatty acid metabolism, and 1 was involved in DNA repair (Table 2-C). Among genes specific to endothelial exposure, acute phase protein and cytoskeleton associated gene were up-regulated. Down-regulated genes were associated with signal transduction, protein trafficking and DNA repair (Table 2-D). In contrast to cell specific exposure groups, the genes with altered expression by neutrons or γ-rays were small in number and did not appear to possess significantly different characteristics (Table 2-E and -F). In each Table, up-regulated genes are presented in decreasing order and down-regulated genes in increasing order. All primary Microarray data are available at the site of GEO (http://www.ncbi.nlm.nih.gov/project/geo/) (data No. GSE9290).

In order to validate the consistency of microarray analysis in the present study, we compared gene expression levels of selected genes between microarray and real-time PCR. We determined the mean value of expression of the selected genes in 5 independent mice from each exposure group. This was compared with those in pooled RNA from 5 non-irradiated mice. The qualitative changes in gene expression levels were consistent between these analyses. However, the quantitative difference was greater in real-time PCR than in microarray analysis, both in up- and down-regulated genes (Table 3).

Since radiation exposure could be hepatotoxic, we compared the results of our present study with the results by McMillian *et al.*[9] They performed microarray analysis of gene expression in rat liver 24 hrs after administration of various kinds of hepatotoxic compounds. We picked up genes whose expression level increased more than 2-fold or decreased to less than 1/2 of the control level in their or our study (Table 4). Over-expression of Mt1 and hemopexin (Hpxn), and under-expression of CYP were prominent in radiation-exposed samples compared with those undergoing administration of hepatotoxic chemical compounds and peroxisome proliferator agonists.

DISCUSSION

Gene array analysis of RNA from irradiated tissues is an effective tool for identifying genes of potential interest in the development of tissue injury. Since Thorotrast naturally emits α-particles and causes liver cancers, evaluating changes in gene expression in the liver irradiated with α-particles might help us to understand how Thorotrasts induce liver cancer. In order to analyze the effect of target cell specificity and quality of irradiation on gene expression in the liver, we intended to separately expose Kupffer and endothelial cells to α-particles using BNC, and performed oligonucleotide microarray analysis. Ishida *et al.* reported that 4 hrs after injection into mice, 5% of bare liposomes and 50% of PEG-liposomes are retained in the blood, respectively, whereas, 70% of bare liposomes and 15% of PEG-liposomes accumulate in the liver, respectively.[10] Assuming that liposomes in either form are phagocytosed by Kupffer cells in the liver, the dose ratio of Kupffer group to endothelial group is 4.7 folds in Kupffer cell group and 1/10 in endothelial cell group in this study. Although we could not completely separate target cells for α-particle exposure, we think these numbers were satisfactory because of internal exposure experiments of the mouse. The cellular responses of Kupffer and endothelial groups were the closest to other groups, whilst the group exposed to neutrons showed greatest variations from other groups (Fig. 2). This suggests that cellular responses are mainly determined by the quality of radiation, that is, dependent on exposure to high LET particles or low LET photons.

Acute phase response refers to changes in concentrations of a number of plasma proteins, termed acute-phase proteins (APPs) which reflect re-orchestration of the pattern of gene

expression in hepatocytes in response to a variety of systemic injuries. An APP has been defined as one whose plasma concentration increases (positive APP) or decreases (negative APP) by at least 25% after injury. In the present study, we detected significant changes of the level of APPs such as Hpxn, ceruloplasmin (Cp) and transthyretin (Ttr) commonly in Kupffer and endothelial exposures (Table 2-B). These indicate that the alterations of gene expression in this study reflect those of hepatocytes even after Kupffer cells and endothelial cells were specifically exposed to α-particles. Cp has a scavenger activity[11] and Hpxn acts as an antioxidant by its strong heme binding and iron homeostasis properties.[12] During inflammation, macrophages and endothelial cells secrete the so-called pro-inflammatory cytokines, tumor necrosis factor-α (TNF-α), Interleukin-1β (IL1β) and IL6.[13] Mt also has antioxidant activity and this gene expression is induced by IL6.[14] Lipocalin is also an APP involved in a mammalian defense mechanism against bacterial infection and works by binding to the iron group within bacterial iron-containing siderophores.[15] Interestingly, acute lung injury in mice induced by lipopolysaccharide and diesel exhaust[16] particles up-regulates lipocalin 2 and Mt2 gene expressions.[16] The present study suggests that pro-inflammatory cytokines are secreted by irradiated macrophages and endothelial cells, especially those exposed to α-particles. Mouse macrophages are activated after whole body irradiation to 4 Gy of γ-rays. However, this activation is not a direct effect of radiation but an indirect effect induced by phagocytosis of apoptotic cells after irradiation.[17] In the present study, the destruction of macrophages and endothelial cells in the spleen was also observed (data not shown). We need to take account of the indirect effects on the spleen of radiation exposure when considering liver carcinogenesis of Thorotrast patients, because the spleen in Thorotrast patients is drastically reduced in size compared to the liver. The changes in gene expression profile commonly observed after Kupffer cell and endothelial cell exposures revealed that hepatocytes are in the state of inflammation and are tending towards proliferation at the cost of metabolic activities. Hepatocytes also actively perform quality control of substances by up-regulation of intracellular protein trafficking.

Expression of genes encoding molecules associated with transcription was up-regulated and expression for those associated with signal transduction was down-regulated in the liver. Further study to characterize molecules involved in these gene expressions would elucidate radiation carcinogenesis, especially that of Thorotrast-induced liver tumors. It is noticeable that *epidermal growth factor receptor* (*EGFR*) and *cyclin E1* gene expressions were up-regulated in the liver whose Kupffer cells or endothelial cells were exposed to α-particles, whereas *xeroderma pigmentosum, complementation group C (XPC)* and *insulin-like growth factor binding protein 2 (IGFBP2)* gene expressions were down-regulated in Kupffer cell irradiated group and *BRAP* gene expression in endothelial cell irradiated group. The level of *EGFR* gene expression in tumors has been correlated to the degree of radiation resistance.[18] Exposure of the breast cancer cell line, MCF-7 to γ-rays enhanced EGFR gene expression concomitant with overexpression of its ligand, TGFα,[19] resulting in enhanced cell growth by irradiation.[20] Recently, new targets for cancer treatment have been identified in head and neck squamous cell carcinomas (HNSCC) as playing key roles in tumor proliferation and metastasis. The first one led to the approval of a molecularly based therapy in HNSCC is EGFR.[21] Cyclin E initiates cells to pass from G1- to S-phase and controls genomic stability. High level expression of cyclin E has been associated with the initiation or progression of various human cancers.[22] Transgenic mice in which cyclin E is constitutively expressed develop malignant diseases, supporting the notion of cyclin E as a dominant onco-protein.[23] XPC carries out the first step of global genome repair in nucleotide excision repair. The lack of the XPC protein is associated with UV-induced skin tumors but not with hypersensitivity against ionizing radiation.[24] IGFBP2 in breast cancer cell lines is a marker of resistance against anti-estrogen therapy.[25] It has also been shown that IGFBP2 plays a key role in the activation of the Akt pathway and collaborates with K-Ras or platelet-derived growth factor beta polypeptide (PDGFB) in the development and progression of two major types of glioma.[26] These results suggest that irradiated liver is in the condition toward cancer induction.

Comparison with the data of McMillian *et al.*[9] revealed that all types of radiation exposure investigated involve macrophage activation rather than peroxisome proliferation (Table 4). Up-regulations of Mt1 and Hpxn, and down-regulation of CYP and retinol binding protein 4 (Rbp4) are characteristic of radiation exposure. Steatohepatitis including alcoholic fatty liver is well known to be a precursor status toward liver fibrosis and liver cancer. Since diverse causes of steatohepatitis are characterized by increased mitochondrial (mt) reactive oxygen species (ROS) production, limited repair of mtDNA and accumulation of oxidatively damaged DNA,[27] cellular reaction against radiation toward lipogenesis may indirectly contribute to DNA insult by high LET radiation. Therefore, intensive or preventive anti-inflammatory treatment could help radiation-induced injury. Most of the genes involved in ATP synthesis, oxidative phosphorylation, copper ion homeostasis and electron transport were induced by both continuous and acute exposure of *Saccharomyces cerevisiae* to γ-rays.[28] The results were concordant with the present study though we focused on *in vivo* radiation of the mouse liver. Furthermore, it has been shown that microvascular endothelial cells are the primary target to initiate intestinal radiation damage.[29] These similarities indicate that cell-to-cell interaction in response to radiation *in vivo* is the result of amplification of *in vitro*

signals. In order to separate the effects of irradiation on parenchymal, Kupffere and endothelial cells, experiments involving irradiation of these cell types after cell fractionation are underway in our laboratory.

ACKNOWLEDGEMENTS

This study was supported in part by the Grants-in Aid from the Ministry of Education, Science, Sports and Culture and the Ministry of Health, Labor and Welfare of Japan. We thank Shoko Ono for her technical assistance.

REFERENCES

1. Goto, A., Takebayashi, Y., Liu, D., Li, L., Saiga, T., Mori, T., Yamadera, A. and Fukumoto, M. (2002) Microdistribution of alpha particles in pathological sections of tissues from thorotrast patients detected by imaging plate autoradiography. Radiat Res. **158**: 54–60.
2. Sharp, G. B. (2002) The relationship between internally deposited alpha-particle radiation and subsite-specific liver cancer and liver cirrhosis: an analysis of published data. J Radiat Res. **43**: 371–380.
3. Ober, S., Zerban, H., Spiethoff, A., Wegener, K., Schwarz, M. and Bannasch, P. (1994) Preneoplastic foci of altered hepatocytes induced in rats by irradiation with alpha-particles of Thorotrast and neutrons. Cancer Lett. **83**: 81–88.
4. Kopp-Schneider, A., Haertel, T., Burkholder, I., Bannasch, P., Wesch, H., Groos, J. and Heeger, S. (2006) Investigating the formation and growth of alpha-particle radiation-induced foci of altered hepatocytes: a model-based approach. Radiat Res. **166**: 422–430.
5. Yuda, T., Pongpaibul, Y., Maruyama, K. and Iwatsuru, M. (1999) Activity of Amphipathic Polyethyleneglycols to Prolong the Circulation Time of Liposomes. Journal of Pharmaceutical Science and Technology, Japan. **59**: 32–42.
6. Weichselbaum, R. R., Hallahan, D. E., Sukhatme, V., Dritschilo, A., Sherman, M. L. and Kufe, D. W. (1991) Biological consequences of gene regulation after ionizing radiation exposure. J Natl Cancer Inst. **83**: 480–484.
7. Maruyama, K., Ishida, O., Kasaoka, S., Takizawa, T., Utoguchi, N., Shinohara, A., Chiba, M., Kobayashi, H., Eriguchi, M. and Yanagie, H. (2004) Intracellular targeting of sodium mercaptoundecahydrododecaborate (BSH) to solid tumors by transferrin-PEG liposomes, for boron neutron-capture therapy (BNCT). J Control Release. **98**: 195–207.
8. Ward, J. H., (1963) Hierarchical Grouping to Optimize an Objective Function. J. Am. Statist. Assoc. **58**: 236–244.
9. McMillian, M., Nie, A. Y., Parker, J. B., Leone, A., Kemmerer, M., Bryant, S., Herlich, J., Yieh, L., Bittner, A., Liu, X., Wan, J. and Johnson, M. D. (2004) Inverse gene expression patterns for macrophage activating hepatotoxicants and peroxisome proliferators in rat liver. Biochem Pharmacol. **67**: 2141–2165.
10. Ishida, O., Maruyama, K., Sasaki, K. and Iwatsuru, M. (1999) Size-dependent extravasation and interstitial localization of polyethyleneglycol liposomes in solid tumor-bearing mice. Int J Pharm. **190**: 49–56.
11. Goldstein, I. M., Kaplan, H. B., Edelson, H. S. and Weissmann, G. (1982) Ceruloplasmin: an acute phase reactant that scavenges oxygen-derived free radicals. Ann N Y Acad Sci. **389**: 368–379.
12. Delanghe, J. R. and Langlois, M. R. (2001) Hemopexin: a review of biological aspects and the role in laboratory medicine. Clin Chim Acta. **312**: 13–23.
13. Trey, J. E. and Kushner, I. (1995) The acute phase response and the hematopoietic system: the role of cytokines. Crit Rev Oncol Hematol. **21**: 1–18.
14. Davis, S. R. and Cousins, R. J. (2000) Metallothionein expression in animals: a physiological perspective on function. J Nutr. **130**: 1085–1088.
15. Flo, T. H., Smith, K. D., Sato, S., Rodriguez, D. J., Holmes, M. A., Strong, R. K., Akira, S. and Aderem, A. (2004) Lipocalin 2 mediates an innate immune response to bacterial infection by sequestrating iron. Nature. **432**: 917–921.
16. Yanagisawa, R., Takano, H., Inoue, K., Ichinose, T., Yoshida, S., Sadakane, K., Takeda, K., Yoshino, S., Yamaki, K., Kumagai, Y. and Yoshikawa, T. (2004) Complementary DNA microarray analysis in acute lung injury induced by lipopolysaccharide and diesel exhaust particles. Exp Biol Med (Maywood). **229**: 1081–1087.
17. Lorimore, S. A., Coates, P. J., Scobie, G. E., Milne, G. and Wright, E. G. (2001) Inflammatory-type responses after exposure to ionizing radiation *in vivo*: a mechanism for radiation-induced bystander effects? Oncogene. **20**: 7085–7095.
18. Ochs, J. S. (2004) Rationale and clinical basis for combining gefitinib (IRESSA, ZD1839) with radiation therapy for solid tumors. Int J Radiat Oncol Biol Phys. **58**: 941–949.
19. Schmidt-Ullrich, R. K., Valerie, K. C., Chan, W. and McWilliams, D. (1994) Altered expression of epidermal growth factor receptor and estrogen receptor in MCF-7 cells after single and repeated radiation exposures. Int J Radiat Oncol Biol Phys. **29**: 813–819.
20. Hagan, M., Yacoub, A. and Dent, P. (2004) Ionizing radiation causes a dose-dependent release of transforming growth factor alpha *in vitro* from irradiated xenografts and during palliative treatment of hormone-refractory prostate carcinoma. Clin Cancer Res. **10**: 5724–5731.
21. Le Tourneau, C., Faivre, S. and Siu, L. L. (2007) Molecular targeted therapy of head and neck cancer: Review and clinical development challenges. Eur J Cancer.
22. Donnellan, R. and Chetty, R. (1999) Cyclin E in human cancers. Faseb J. **13**: 773–780.
23. Moroy, T. and Geisen, C. (2004) Cyclin E. Int J Biochem Cell Biol. **36**: 1424–1439.
24. Arlett, C. F., Plowman, P. N., Rogers, P. B., Parris, C. N., Abbaszadeh, F., Green, M. H., McMillan, T. J., Bush, C., Foray, N. and Lehmann, A. R. (2006) Clinical and cellular ionizing radiation sensitivity in a patient with xeroderma pigmentosum. Br J Radiol. **79**: 510–517.
25. Juncker-Jensen, A., Lykkesfeldt, A. E., Worm, J., Ralfkiaer, U., Espelund, U. and Jepsen, J. S. (2006) Insulin-like growth factor binding protein 2 is a marker for antiestrogen resistant human breast cancer cell lines but is not a major growth regulator. Growth Horm IGF Res. **16**: 224–239.

26. Dunlap, S. M., Celestino, J., Wang, H., Jiang, R., Holland, E. C., Fuller, G. N. and Zhang, W. (2007) Insulin-like growth factor binding protein 2 promotes glioma development and progression. Proc Natl Acad Sci USA. **104**: 11736–11741.
27. Gao, D., Wei, C., Chen, L., Huang, J., Yang, S. and Diehl, A. M. (2004) Oxidative DNA damage and DNA repair enzyme expression are inversely related in murine models of fatty liver disease. Am J Physiol Gastrointest Liver Physiol. **287**: G1070–1077.
28. Mercier, G., Berthault, N., Mary, J., Peyre, J., Antoniadis, A., Comet, J. P., Cornuejols, A., Froidevaux, C. and Dutreix, M. (2004) Biological detection of low radiation doses by combining results of two microarray analysis methods. Nucleic Acids Res. **32**: e12.
29. Paris, F., Fuks, Z., Kang, A., Capodieci, P., Juan, G., Ehleiter, D., Haimovitz-Friedman, A., Cordon-Cardo, C. and Kolesnick, R. (2001) Endothelial apoptosis as the primary lesion initiating intestinal radiation damage in mice. Science. **293**: 293–297.

Received on August 16, 2007
Revision received on October 11, 2007
Accepted on October 18, 2007
J-STAGE Advance Publication Date: November 30, 2007

Novel SN-38–Incorporated Polymeric Micelle, NK012, Strongly Suppresses Renal Cancer Progression

Makoto Sumitomo,[1] Fumiaki Koizumi,[2] Takako Asano,[1] Akio Horiguchi,[1] Keiichi Ito,[1] Tomohiko Asano,[1] Tadao Kakizoe,[3] Masamichi Hayakawa,[1] and Yasuhiro Matsumura[4]

[1]Department of Urology, National Defense Medical College, Tokorozawa, Saitama, Japan; [2]Shien-Lab, Medical Oncology, National Cancer Center Hospital; [3]National Cancer Center, Tokyo, Japan; and [4]Investigative Treatment Division, Research Center for Innovative Oncology, National Cancer Center Hospital East, Chiba, Japan

Abstract

It has been recently reported that NK012, a 7-ethyl-10-hydroxy-camptothecin (SN-38)–releasing nanodevice, markedly enhances the antitumor activity of SN-38, especially in hypervascular tumors through the enhanced permeability and retention effect. Renal cell carcinoma (RCC) is a typical hypervascular tumor with an irregular vascular architecture. We therefore investigated the antitumor activity of NK012 in a hypervascular tumor model from RCC. Immunohistochemical examination revealed that Renca tumors contained much more CD34-positive neovessels than SKRC-49 tumors. Compared with CPT-11, NK012 had significant antitumor activity against both bulky Renca and SKRC-49 tumors. Notably, NK012 eradicated rapid-growing Renca tumors in 6 of 10 mice, whereas it failed to eradicate SKRC-49 tumors. In the pulmonary metastasis treatment model, an enhanced and prolonged distribution of free SN-38 was observed in metastatic lung tissues but not in nonmetastatic lung tissues after NK012 administration. NK012 treatment resulted in a significant decrease in metastatic nodule number and was of benefit to survival. Our study shows the outstanding advantage of polymeric micelle-based drug carriers and suggests that NK012 would be effective in treating disseminated RCCs with irregular vascular architectures. [Cancer Res 2008;68(6):1631–5]

Introduction

Passive targeting of the drug delivery system is suited to combating the pathophysiologic characteristics present in many solid tumors: hypervascularity, irregular vascular architecture, potential for secretion of vascular permeability factors, and the absence of effective lymphatic drainage that prevents efficient clearance of macromolecules. These characteristics, unique to solid tumors, are believed to be the basis of the enhanced permeability and retention (EPR) effect (1). Polymeric micelle-based anticancer drugs have recently been developed (2, 3), and some were put under evaluation for clinical trials (4, 5).

7-Ethyl-10-hydroxy-camptothecin (SN-38), a biological active metabolite of irinotecan hydrochloride (CPT-11), has potent antitumor activity, but has not been used clinically because it is a water-insoluble drug. It has been recently shown that novel SN38-incorporated polymeric micelles, NK012, have the potential to allow effective sustained release of SN-38 inside a tumor and possess potent antitumor activities especially in a vascular endothelial growth factor (VEGF)–secreting hypervascular tumor (6), because the supramolecular structures of NK012 which enable SN-38 to accumulate in the target tissue are based on the EPR effect (1).

Renal cell carcinoma (RCC) is a typical hypervascular tumor with an irregular vascular architecture. We therefore conducted an investigation to determine whether NK012 would be effective in treating RCC by using established RCC tumor models with pulmonary metastasis.

Materials and Methods

Drugs and cells. CPT-11 was purchased from Yakult Honsha Co., Ltd. SN-38 and NK012 was prepared and supplied by Nippon Kayaku Co., Ltd. (6). Five human RCC lines (SKRC-49, Caki-1, 769P, 786O, and KU19-20) and murine Renca cells were maintained in DMEM or MEM supplemented with 2 mmol/L glutamine, 1% nonessential amino acids, 100 units/mL streptomycin and penicillin, and 10% FCS.

***In vitro* growth inhibition assay.** The growth inhibitory effects of NK012, SN-38, and CPT-11 were examined with a 3-(4, 5-dimethylthiazol-2-yl)-2, 5-diphenyltetrazolium bromide (MTT) assay, as described previously (6).

***In vivo* growth inhibition assay.** The animal experimental protocols were approved by the Committee for Ethics of Animal Experimentation, and the experiments were conducted in accordance with the Guidelines for Animal Experiments in the National Cancer Center. Athymic nude mice (3–4 wk old) were maintained in a laminar air flow cabinet under aseptic conditions. 10^7 RCC cells were s.c. injected into the backs of the mice. NK012 at doses of 10 mg/kg/d or 20 mg/kg/d and CPT-11 at doses of 15 mg/kg/d or 30 mg/kg/d were given i.v. on days 0 (when tumors were allowed to grow until they became massive in size, around 1.5 cm), 4, and 8. Tumor volume was determined by direct measurement with calipers and calculated as $\pi/6 \times (\text{large diameter}) \times (\text{small diameter})^2$.

Assessment of treatment effects of NK012 on murine pulmonary metastasis model. A total of 1×10^5 Renca cells were inoculated into male BALB/c mice via the tail vein. The mice were randomly divided into three groups of 10. NK012 at dose of 20 mg/kg/d and CPT-11 at dose of 30 mg/kg/d were given i.v. on days 0 (7 d after inoculation), 4, and 8. After that, the mice were sacrificed, their lungs were stained intratracheally with 15% India black ink solution, and the number of metastatic nodules in each mouse was counted. To determine the effect of NK012 on survival, an identical experiment to the one described above was done. After treatment, mice were maintained until each animal showed signs of morbidity (i.e., over 10% weight loss compared with untreated controls), at which point they were sacrificed. Kaplan-Meier analysis was done to determine the effect on time to morbidity, and statistical differences were ranked according to a Mantel-Cox log-rank test using the StatView 5.0 software package.

Histologic and immunohistochemical analysis. Histologic sections were taken from Renca tumor tissues. After extirpation, tissues were fixed with 3.9% formalin in PBS (pH 7.4), and the subsequent preparations and H&E staining were performed by Tokyo Histopathological Laboratory Co.,

Requests for reprints: Yasuhiro Matsumura, Investigative Treatment Division, Research Center for Innovative Oncology, National Cancer Center Hospital East, 6-5-1 Kashiwanoha, Kashiwa City, Chiba 277-8577, Japan. Phone: 81-4-7134-6857; Fax: 81-4-7134-6857; E-mail: yhmatsum@east.ncc.go.jp.

doi:10.1158/0008-5472.CAN-07-6532